Master Thesis

Process modelling for Model Predictive Control of Incremental Sheet Forming

D.B. (Dylan) Sikkelbein

January 2021

Mechanical Engineering
Chair of Nonlinear Solid Mechanics

Graduation committee:
Prof. dr. ir. A.H. van den Boogaard (chairman)
Dr. ir. G.T. Havinga (daily supervisor)
Dr. ir. W.B.J. Hakvoort (external member)

UNIVERSITY OF TWENTE.

Abstract

Incremental Sheet Forming is a promising flexible sheet forming process that is flawed by its geometric accuracy. A process model can be used to steer the process to its target, but it is difficult to determine a good model due to the non-linearity of forming processes. In this work, it is investigated what types of linearised models can be created for closed-loop control of ISF, and to what extent such models are valid. The models are determined based on FE models, which are also used to investigate the validity of the linearisations, and to test the performance of the controllers. Extensions to existing process models were made and tested on both a simple cone and a more complex two-angle pyramid. The extensions proved to capture some of the non-linearities in the process and increase the performance of the control system.

Keywords: Incremental Sheet Forming, Model Predictive Control, Toolpath Linearisation

Preface

This thesis concludes the master programme Mechanical Engineering and with that my 5½ years of studying at the University of Twente. A time that I thoroughly enjoyed and in which I was able to develop myself from someone who was good in math and physics to an engineer.

Research is never done truly by one person alone. Therefore I would like to thank a few people. When doing research, I always appreciate feedback from experienced people in the field. I would like to thank Professor Joost Duflou and Hans Vanhove from KU Leuven, which gave me a good overview of the process fundamentals and common problems in Incremental Sheet Forming. Furthermore I would like to thank Professor Stephan Duncan from the University of Oxford for feedback on the control theory in this work.

During the last 9 months I could rely on the guidance and closed-loop feedback of my supervisor Jos Havinga. While we never met in person during my graduation due to the Covid-19 pandemic, I was pleased with the way in which we could have vivid discussions and explore ideas on how to approach problems. Thank you for making a lot of time for that.

Last but not least I would like to thank my family and especially my girlfriend for their support. Thank you Chantal for taking up the positions of colleague, coffee and cake caterer, lunch walk buddy, decision maker for plot colours, but above all loving girlfriend in these work-at-home times.

Enschede, January 2021,
Dylan Sikkelbein

Contents

Glossaries

Control action	Output of the controller. In this thesis often a correction on the nominal step height between contours (Δu) or radial step between contours (Δv).
Process state	In its most general form, the complete state of the product (stresses, strains, etc.). In this thesis, the evaluated state is often only the deflection perpendicular to the flat sheet.
Process model	Model that predicts the state of the process over time as a result of the process input.
Control model	In this work, the term that predicts the effect of control actions in the process model is referred to as the Control model.
Nominal path	Path that is followed if no control is applied. The "path" refers to vertical step height or radial step between the contours.
Nominal state	State of the part as a result of following the nominal path.
State evolution	Change state over a number of time steps.
Nominal state evolution	Change of state over time when the nominal path is followed.

Symbols

$\boldsymbol{\Omega}$	Space occupied by the product
$\boldsymbol{x}$	Spatial discretization points
t	Time [s]
$\boldsymbol{z}$	Considered product state
$\boldsymbol{Z}$	Full product state
$\bar{[\cdot]}$	Nominal value
$\hat{[\cdot]}$	Target value
$\tilde{[\cdot]}$	Predicted value
$\boldsymbol{u}$	Depth increments
$\Delta\boldsymbol{u}$	Depth increment corrections
$\boldsymbol{v}$	Radial increments
$\Delta\boldsymbol{v}$	Radial increment corrections
$\boldsymbol{G}$	Response matrix, effect of control actions $\Delta\boldsymbol{u}/\Delta\boldsymbol{v}$
$\boldsymbol{Q}$	Response matrix when both future and past control actions are accounted for
$[\cdot]^i$	At location i
$[\cdot]_k$	At time k
$[\cdot]_{his}$	Corresponding to time steps in the past
$[\cdot]_{opt}$	Corresponding to time steps in the future
$[\cdot](\Delta u_k)$	Corresponding to an analysis in which a single control action Δu is applied at step k

Acronyms

ISF	Incremental Sheet Forming
SPIF	Single Point Incremental Forming
QP	Quadratic Programming
MPC	Model Predictive Control
ILC	Iterative Learning Control
CNC	Computer Numerical Control

Scalars are denoted by non-bold lowercase Roman letters (a). Vectors by bold lowercase Roman letters ($\boldsymbol{a}$). Matrices in bold capital Roman letters ($\boldsymbol{A}$). The rows or columns of matrix $\boldsymbol{A}$ are denoted by a subscript ($\boldsymbol{a}_i$). In the case of time-varying matrices and vectors, the time-variance is denoted by subscript k ($\boldsymbol{A}_k$).

1 Introduction

Today we are in what many consider the fourth industrial revolution. The connectivity between systems and machines paves the way for mass customization in smart factories [1]. Conventional sheet metal forming processes such as stamp forming are unsuitable for mass-customization as they require dedicated die sets for each product.

Over the last few decades, many flexible forming processes have been proposed. An example is a re-configurable die in stamp forming. A matrix of punches with hemispherical tips can mimic the surface of a conventional die. However, this process has not been widely adopted by the industry due to poor surface quality of the product [2].

This thesis will focus on another set of flexible forming processes called incremental sheet forming (ISF). This type of processes is characterized by the accumulation of local deformation in subsequent increments. The most simple variant is single-point incremental sheet forming (SPIF), in which a single hemispherical tool moves over the surface of a fully clamped sheet (fig. 1.1a). The first patents on SPIF originate from the last decade of the previous century [3].

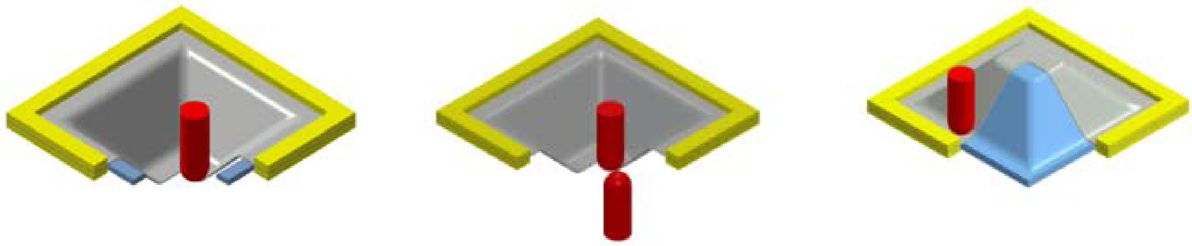

(a) Single Point Incremental Forming (SPIF)

(b) Double Sided Incremental Forming (DSIF)

(c) Two point incremental forming (full die)

Figure 1.1: Process variations of incremental sheet forming [4]

Even after nearly two decades of extensive research, ISF has not been fully adapted by the industry yet. This is mainly due to its poor geometric accuracy caused by elastic springback and global bending due to the lack of support. Other variants of ISF with additional support have been developed to improve accuracy. Double Sided Incremental Forming (DSIF, fig. 1.1b) provides additional support with a second tool on the opposite side of the sheet to prevent global bending. Some other variants make use of a partial or full die to provide more support (fig. 1.1c).

The most common way to account for the lack of accuracy in ISF is tool path optimization. If the effect of toolpath corrections on the final geometry of the product can be well predicted in a process model, the toolpath can be optimized such that the geometric error is minimal. However, the non-linearity of metal forming processes makes the definition of a process model difficult. Finite Element models can be used to model the process, but the large simulation times of hours to days make them unsuitable to determine full non-linear process models. For real-time control, processing times in the order of seconds are desirable.

Research on SPIF is mainly done with simple and small geometries. In theory every geometry that can be achieved in regular sheet metal forming could be formed by ISF. Possibly even more complex geometries are possible because of the degrees of freedom that robot manipulators facilitate. Since flexible metal forming processes do not require investment in dies, they are particularly suitable for one-of-a-kind products or small batches and extremely large products for which producing dies is not feasible. For example, Duflou et al. [5] and Ambrogio et al. [6] used ISF to manufacture patient-specific titanium prostheses (fig. 1.2a), the Amino corporation [7] explored the use of ISF to produce rare products and manufactured a replacement hood for a Honda S800 Oldtimer (fig. 1.2b) and Hirt et al. [8] researched whether ISF can lower the costs per part of an A320 door panel, which would otherwise require multiple production steps (fig. 1.2c).

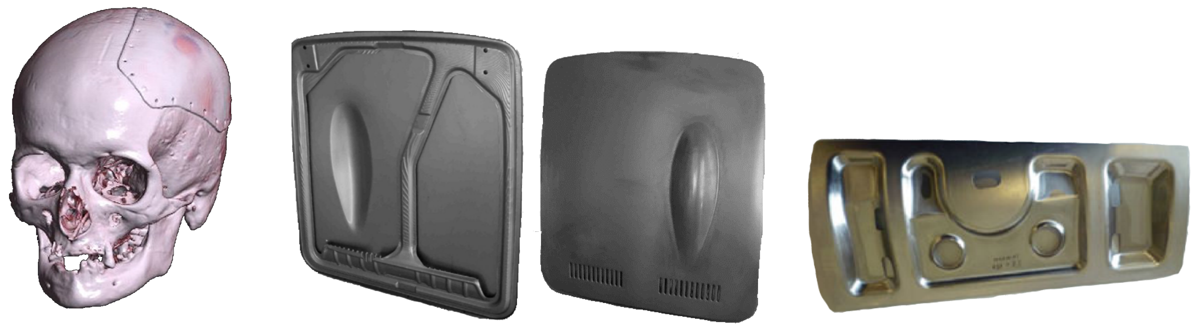

(a) Skull implant [5] **(b)** Honda S800 hood [7] **(c)** A320 door panel [8]

Figure 1.2: Incremental Sheet Forming Applications

1.1 Problem description

This thesis investigates the definition of the process model used in tool path optimization of incremental sheet forming and its performance in Model Predictive Control (MPC). The following subjects will be discussed:

Process linearisation Since the complete non-linearity of the process is impossible to capture, it is desirable to simplify the process by linearisation. In this linearisation it is assumed that small corrections on the toolpath have a linear effect on the geometry. Questions here are how these models should be determined and to what extent the assumption of linearity is valid.

MPC performance Besides the accuracy of the linearised model, it is of importance how such a model affects the MPC controller in terms of stability and robustness. The linearisations developed in this thesis will be tested on an Incremental Sheet Forming Process simulated using a Finite Element model.

This thesis is structured as follows. Chapter 2 includes a literature review on ISF, control in metal forming in general and the use of Model Predictive Control in ISF. Chapter 3 contains the theory on the new models developed in this thesis. In Chapter 4, the theory is applied on an axisymmetric geometry to test the fundamentals on a simple and insightful product, after which the performance of the new models is tested on a more complex product in Chapter 5. Conclusions and recommendations will be given in Chapter 6.

2 | Literature Review

2.1 Incremental sheet forming

Research on ISF ranges from practical research on toolpath generation, accuracy improvement and equipment use to more fundamental research in metallurgy, solid mechanics and process control. Only the research relevant for the understanding of accuracy improvement of Single Point Incremental Sheet forming (SPIF) will be mentioned here.

2.1.1 Process fundamentals

The lack of support in SPIF makes the process very different from conventional sheet metal forming. While the degrees of freedom of the tool and ability to steer the process during manufacturing give possibilities for process control, some sources of geometric error in SPIF are hard to overcome. Lu et al. [9] identified three causes of geometric error in the incremental forming of a truncated cone: global bending of the sheet due to the lack of support, the pillow effect due to compressive stresses in the bottom of the cup and elastic springback of the whole cup (see fig. 2.1). Ren et al. [10] also mentioned springback of the part during unclamping due to residual stresses. This source of error will not be discussed in this thesis.

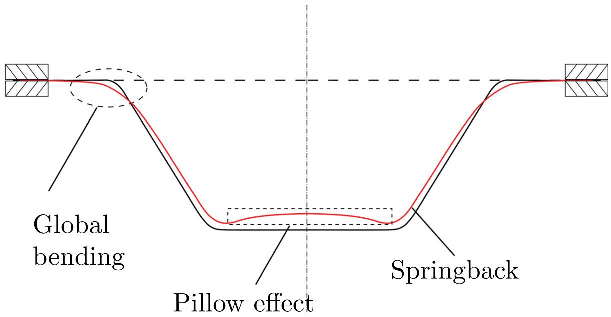

Figure 2.1: Causes of geometric inaccuracy in incremental sheet forming [9]

2.1.2 Accuracy improvement

Improving the geometric error can generally be done in three ways: by modifying the material, by providing additional support and by toolpath optimization.

Material modification

Hot forming is a well-known solution to increase formability and reduce tool force and springback [11]. The actual use of it is however expensive. The local nature of ISF makes that the heating can be concentrated on the forming region around the tool. Therefore, attempts of combining local heating and ISF have been done to increase formability and reduce springback. Duflou et al. [12] developed laser assisted SPIF by heating up the blank on the opposite side of the sheet than where the tool is and observed higher formability and less springback. Fan et al. [13] developed a similar process but used high currents to produce heat instead. Their Electric hot incremental forming process led to accuracy improvement but the high current severely affected the surface finish and resulting accuracy on a small scale. The strategy worked especially well in reducing the bulging of flat walls surfaces.

Additional support

The lack of dies in ISF is one of its key selling points. The geometric inaccuracies caused by the lack of dies are however so large that a form of additional support is desirable. A simple solution would be to place a (partial) die on one side of the product. The local deformation in ISF causes much lower process forces than in regular stamping, which allows the use of cheap materials as wood or resin for dies [14]. A more advanced strategy to provide additional support is Double Sided Incremental sheet forming. In this process a second tool provides the support on the other side of the material. This requires a second CNC setup or industrial robot, but retains the flexibility of ISF.

Toolpath optimization

The most common way to account for geometric error is tool path optimization. The freedom of choice in the toolpath and direct effect on the deformation makes it an attractive choice for optimization. Because the earliest research on ISF was done on existing CNC-based setups, the available CAM software was often used to construct a toolpath. These software packages calculate the toolpath by offsetting the target geometry with the tool radius. This strategy does not account for springback or other unwanted deformations and therefore yields inaccurate results.

Improvements can be made by mapping the error of the final geometry to the target geometry. This way, the CAM software packages can still be used. If error mapping is done from product to product iteratively, the strategy can be seen as iterative learning control. Hirt et al. [15] and later Fiorento et al. [16] were the first to exploit this strategy and showed significant improvements within a few iterations. The drawback of this strategy is that multiple experiments have to be done on a single product before a satisfying accuracy is reached, which is conflicting with the flexibility of ISF. Fiorento et al. [17] recently made an effort to get over this drawback by running the first few iterations numerically. Fischer et al. [18] explored the use of multiple ILC iterations on the same product. The error due to springback means that some additional forming is required, which can be done using an ILC iteration. This method proved to be less time-consuming and more cost-effective but failed to reach the same accuracy since over-forming can not be corrected.

Behera et al. [19] proposed a more advanced form of toolpath optimization which recognizes features in the CAD model and corrects the toolpath accordingly. Experiments containing the separate features were used as training sets in a multivariate adaptive regression splines (MARS) model. One of the drawbacks of this approach is that the compensated geometry can contain large wall angles that lead to failure. Especially in the case that the target geometry already contains steep wall angles close to the critical wall angle that causes failure.

2.2 Control in metal forming

The aforementioned forms of toolpath optimization do not involve state feedback and are therefore forms of open-loop control. To deal with uncertainties in the process, closed-loop control with the use of state feedback is desirable.

2.2.1 Uncertainty in metal forming

In many production processes, forms of closed-loop control are already in use. Closed-loop control uses feedback of sensor data to steer the process state towards a target. The use of a control system is required due to different sources of uncertainty in the process:

- **Model error** The process models used to describe the physics in a system are a simplification or approximation of reality. For example, a finite element model can contain numerical error or a material model could be a severe simplification of the actual material characteristics.

- **Disturbances** The process models are often based on a set of parameters which have a certain variance in reality. Fluctuations in material properties, sheet thickness or ambient temperature can affect the outcome of a process, but also make the process model less accurate, which affects the performance of a control system.

- **Measurement error** Closed-loop control makes use of sensor data to steer the process to a target. This sensor data may contain noise or could be poorly calibrated. Also, when indirect measurements are used, for example a force to predict another process state, the estimator that determines their relation can contain its own model error. These sources of uncertainty affect the closed-loop performance of the control system.

Closed-loop control can be applied during the process of a single product, called on-line closed-loop control, or from product to product in a batch, called off-line closed-loop control. The difference is schematically illustrated in fig. 2.2. On-line closed-loop control makes use of workpiece sensors that measure during the process, steering the process during its execution, while off-line closed loop control uses measurements of finished products only. Off-line control can deal with variations between batches of products and disturbances that only occur after the process is finished, such as unclamping or cooling, where on-line control can control the product during manufacturing to account for model error and disturbances.

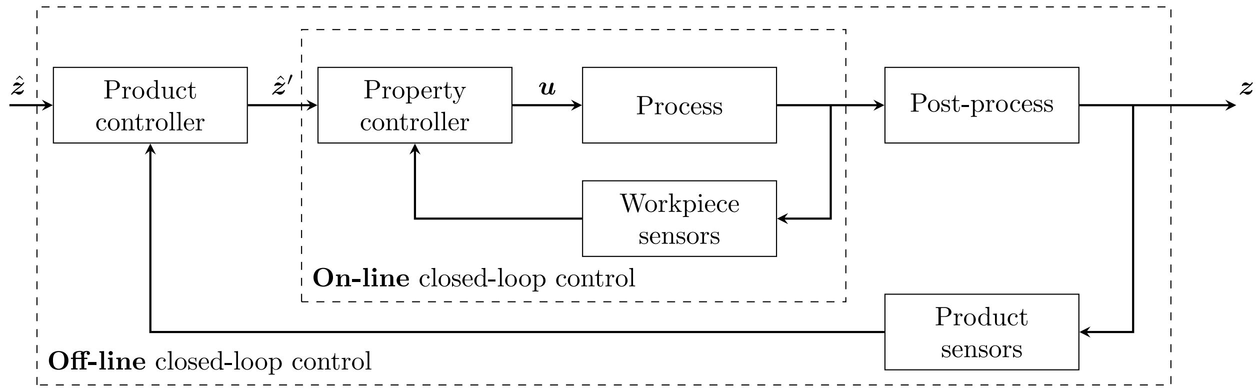

Figure 2.2: Off-line and On-line closed-loop control of product properties, where $\hat{\boldsymbol{z}}$ is the target state, $\hat{\boldsymbol{z}}'$ is the new target state optimized by the product controller and $\boldsymbol{u}$ is the process control input. Adapted from [20].

2.2.2 Model Predictive Control

When a good process model is available, Model Predictive Control (MPC) can be used to optimize the control input in a system. MPC is a control technique that originates from the chemical process industry. Other well-known applications are climate control and vehicle path following systems. MPC relies on a model of the system to optimize all control actions to be made over a certain number of time steps in the future, the finite horizon. In contrary to a continuous chemical process, ISF is finite by nature, so a MPC often optimizes for all control actions to be done yet. After determining all optimal control actions, the first control action is applied. After each new set of measurements, the MPC runs again to perform a new optimisation of all future control actions. The advantage of MPC is that it anticipates on future events and deals with uncertainty by recalculating the optimal strategy on every time instance.

Model Predictive Control in ISF

In control of ISF, MPC can be used to minimize the final geometry error. The considered state $\boldsymbol{z}$ will be the deflection perpendicular to the flat sheet. The control actions will be path corrections $\Delta\boldsymbol{u}$. The controller optimizes the path corrections to be made by minimizing the difference between the target geometry and the geometry predicted by the process model. When time is discretized to N_t steps and the model predictive controller is used at time step k, it solves the following optimization problem:

$$\begin{aligned} \underset{\Delta\boldsymbol{u}}{\text{minimize}} \quad & \|\tilde{\boldsymbol{z}}_{N_t} - \hat{\boldsymbol{z}}_{N_t}\|_2 + \alpha\|\Delta\boldsymbol{u}_k\|_2 \\ \text{subject to} \quad & \tilde{\boldsymbol{z}}_{N_t} = f(\boldsymbol{z}_k, \Delta\boldsymbol{u}_k), \\ & lb \leq \Delta u_i \leq ub \quad \forall\ i \end{aligned} \tag{2.1}$$

Where $\hat{\boldsymbol{z}}_{N_t}$ is the target state and $\tilde{\boldsymbol{z}}_{N_t}$ is the state at the end of the process (time step N_t) as predicted by process model $f(\boldsymbol{z}_k, \Delta\boldsymbol{u}_k)$. The process model predicts the shape of the final geometry according to current state $\boldsymbol{z}_k$ and control actions $\Delta\boldsymbol{u}_k$. The magnitude of the terms in the optimization problem is measured using an euclidean norm ($\|\cdot\|_2$) as described in eq. (4.3). In MPC, the optimization problem will by solved at every time step k, each time accounting for all future time steps that are yet to be performed:

$$\Delta\boldsymbol{u}_k = [\Delta u_k, \Delta u_{k+1}, \ldots, \Delta u_{N_t-1}]^T \tag{2.2}$$

In other words, all corrections Δu after step $k-1$ are optimized such that the difference between the state predicted by the model $\tilde{\boldsymbol{z}}_{N_t}$ and the target $\hat{\boldsymbol{z}}_{N_t}$ is minimal. Additionally, the term $\|\Delta\boldsymbol{u}_k\|_2$ minimizes and smooths the magnitude of the control actions. When $f(\boldsymbol{z}_k, \Delta\boldsymbol{u}_k)$ is a linearized model, this ensures that the linearisation remains valid. The weight of the term that minimizes the magnitude of the control actions is set by α. The optimal value of α depends heavily on the characteristics of the process model and is often determined by trial and error. Lower bound lb and upper bound ub make sure that the critical wall angle and forming limits are not exceeded. Although the complete optimal control strategy over the time horizon is determined, only the control action at current step Δu_k in $\Delta\boldsymbol{u}_k$ is applied in MPC after which the optimization problem is solved at the next time step again. When the process model $f(\boldsymbol{z}_k, \Delta\boldsymbol{u}_k)$ is linear with $\Delta\boldsymbol{u}_k$ the optimization problem is a Quadratic Optimization problem. This problem can be solved efficiently with quadratic programming (QP). The QP formulation used in the MPC is given in appendix B.2

Figure 2.3 shows the steps in closed loop control of a process. In reality the blocks "perform step k" and "measure $\boldsymbol{z}_{k+1}$" are the execution of 1 piece of the discretized toolpath and measurement afterwards. In the numerical environment of this thesis, step k is performed in a Finite Element model, after which the results are post-processed and sent to the MPC in MATLAB.

2.2.3 Including uncertainty in MPC

Robust Model Predictive Control (RMPC) is one of the first attempts to deal with uncertainties in Model Predictive Control. Early formulations were min-max optimization problems in which the worst case scenario of the uncertainty (max) is minimised. This renders the control actions very conservative or even infeasible [21]. Stochastic MPC accounts for model uncertainty and disturbances based on their statistical description.

Polyblank et al. [22] describe briefly how model uncertainty and disturbances can be included mathematically in the standard optimization problem that solves for the corrections to be made. The process models used in control of ISF are more often flawed by systematic errors than stochastic variations. Therefore, this works focusses on reducing model error by making a deterministic description of the error rather than trying to include the stochastic description of the error in the process model.

2.2.4 Current research on MPC in ISF

After Allwood et al. [23] introduced the use of MPC to control ISF, a few extensions have been developed. Wang et al. [24] compared the non-negative least square (NNLQ) and robust least square (RLSQ) optimization strategies in a first attempt to deal with uncertainty.

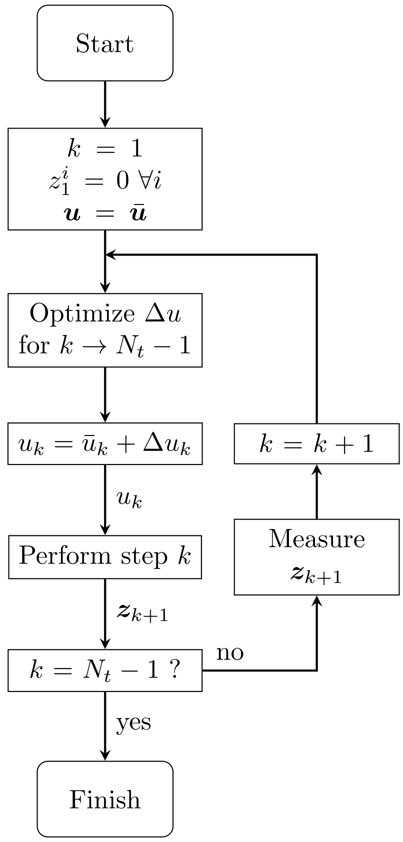

Figure 2.3: Process control scheme for MPC of ISF

He et al. [25] successfully extended the concept of using MPC to non-convex shapes and developed a two-directional MPC which corrects the toolpath both vertically and radially and reduced the error even further than a conventional one-directional MPC [26].

2.3 Control models

In the following chapters, the part of the process model that predicts the effect of control actions is referred to as the control model. This model can be established in different ways. The following sections elaborate on the chosen approach.

2.3.1 Impulse response

In order to control a system, the relation between input and output should be established. In the case of ISF, the input is the tool location and the output is the deformation of the sheet. The non-linearity of metal forming processes makes it difficult to determine the relation between tool location and sheet deformation. Finite Element analysis of processes that evolve over time take hours if not days and the freedom in the choice of toolpath makes that the number of possible inputs is infinitely large. Therefore there is a need for a simplified process model that can accurately capture the relation between tool location and sheet deformation in ISF.

Music and Allwood [27] proposed to characterize ISF with an impulse response in analogy with conventional control theory. If the output of a system can always be predicted with a single linear function, the system is called Linear Time-Invariant (LTI). This single function can be determined by applying an impulse to the system and measuring its response, hence the term impulse response. The output of the system can then be determined by taking the convolution of the input to the system with the system's impulse response. Mathematically, this is written as:

$$\boldsymbol{z}(\boldsymbol{x},t) = \boldsymbol{z}(\boldsymbol{x},0) + \int_0^t \boldsymbol{g}(\boldsymbol{s})u(\tau)\boldsymbol{d}\tau \tag{2.3}$$

Where $\boldsymbol{z}(\boldsymbol{x},t)$ is the state of the system, the deflection of the product normal to the flat sheet, with initial state $\boldsymbol{z}(\boldsymbol{x},0)$. $\boldsymbol{g}$ is the impulse response of the system with $\boldsymbol{s}$ being the distance between material point $\boldsymbol{x}$ and the tool location. u is the input to the system, often the penetration of the tool into the sheet. This approach suits ISF, since the state of the product, the deformation, is the accumulation of deformation caused by the tool as it moves over the surface.

The validity of eq. (2.3) relies on three assumptions:

1. **The impulse response is linear with the control action** The effect of a control action should be linear with its magnitude. Since the impulse response is normalized by the magnitude of the control action, the impulse response should be equal for every magnitude of the control action.

2. **The impulse response is time consistent** The effect of a control action is instantaneous and does not change after future forming steps.

3. **The impulse response is spatially invariant** The impulse response does not vary over the product.

The performance and stability of a control system using eq. (2.3) depends on the extent in which these assumptions hold.

Music and Allwood [27] studied the behavior of the impulse response in ISF by briefly applying the tool to the surface and measuring its response. The results in fig. 2.4 show that the deformation is localized around the tool. The study showed that the impulse response is sufficiently time consistent, linear with the control action and spatially invariant to serve as a simple control model.

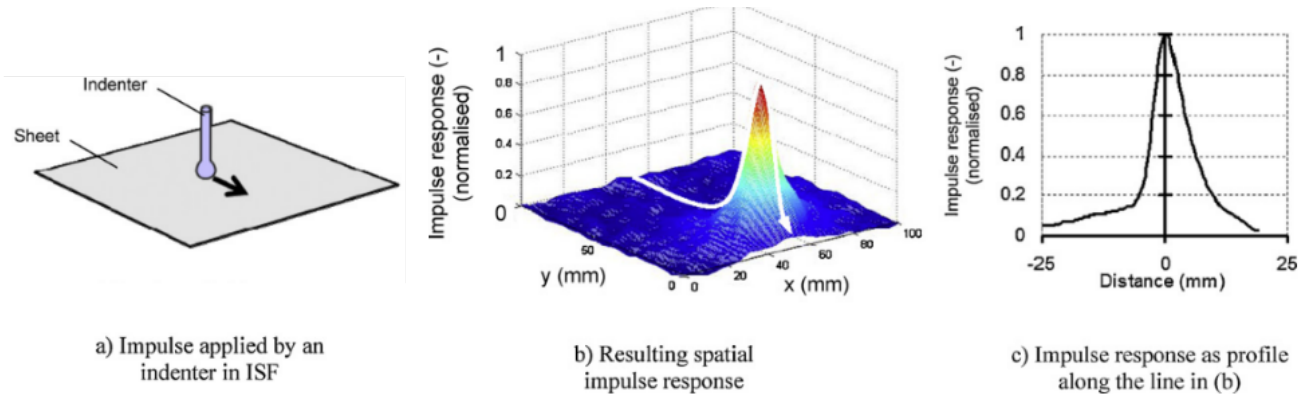

Figure 2.4: Results of the impulse response analysis done by Music and Allwood [27]

The work in this thesis is based on the concept of using impulse response models in model predictive control as developed by Allwood and Music [27].

2.3.2 Control models used in MPC of ISF

Based on the idea of spatial impulse responses, Allwood et al. [23] designed a closed-loop control system to improve the accuracy in ISF. The research was limited to axisymmetric products produced by circular z-level toolpaths. Every circular contour in the toolpath can be described by one radial and height coordinate. The process was discretized in one time step k per contour. A schematic description of this toolpath can be seen in fig. 2.5.

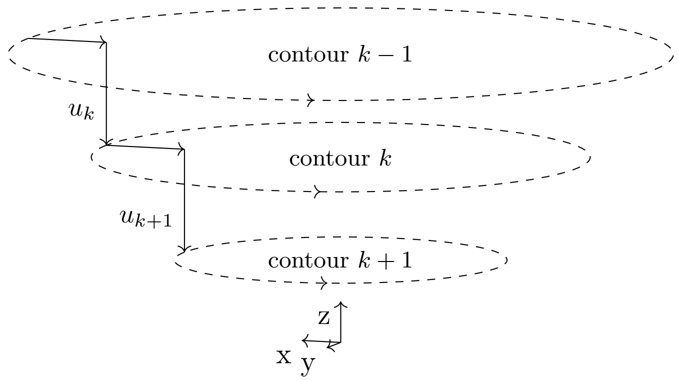

Figure 2.5: Definition of a circular z-level contour toolpath

The impulse response $\boldsymbol{g}$ relates the vertical spacing between the contours u_k to the change in state from $\boldsymbol{z}_k$ to $\boldsymbol{z}_{k+1}$. Note that this has as a result that when a correction on the step height u_k is made at step k, all contours from step k to the last contour will move. The axial symmetry of the products makes it possible to reduce the 3D geometry to a 2D cross-sectional geometry in which the state $\boldsymbol{z}_k$ is a function of the radius, discretized in N_x sampling points. Instead of relating the impulse response to the distance from the tool, the impulse response is now a function of the radial distance, making the impulse response different for each time step k, thus discretizing $\boldsymbol{g}$ to $\boldsymbol{g}_k$ and effectively making the problem a linear time varying (LTV) problem. $\boldsymbol{g}_k$ is defined as:

$$\boldsymbol{g}_k = \frac{\boldsymbol{z}_{k+1} - \boldsymbol{z}_k}{u_k} \tag{2.4}$$

Figure 2.6 shows the shape of the impulse responses early, in the middle of and late in the process. These impulse responses were measured during experiments in which the tool is withdrawn from the surface before measuring. In that case, the product state is the unloaded product geometry and includes springback. The response model in Figure 2.6c contains cumulative Weibull functions fitted on the experimental data in a) and b). Wang et al. [24] also used the cumulative Weibull function as a model in the same process, but related the radial location of the Weibull function to the tool location instead of fitting it to measurements.

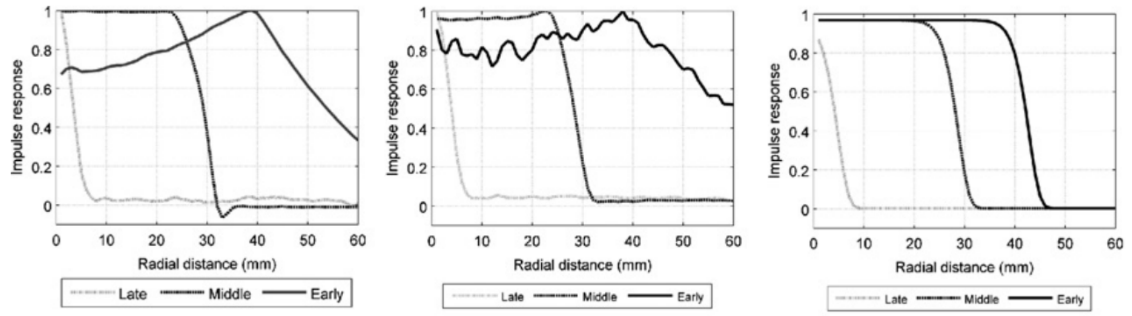

(a) experiments on one-step cone (b) experiments on simple cone (c) analytic approximation using the Weibull survival function

Figure 2.6: Impulse response models as used by Allwood et al. [23]. The responses have been normalized to have a maximum value of 1. A one-step cone contains two wall angles.

A simplification to the Weibull fitted response models is made by Lu et al. [9]. They related the impulse response to the point where the tool tangentially touches the sheet. On radii greater than that point at step $k-1$, the response is zero. On radii smaller than that point at step k, the response is one. In between, it linearly increases from zero to one. This method only uses already available toolpath information and does not require knowledge of the state evolution of the process. It proved to result in reasonable accuracy, both in simple geometries which are reduced to 2D problems as in problems which are spatially discretized over the whole surface of the product [28].

The success of using these control models in Model Predictive Control of ISF depends heavily on the assumptions in section 2.3.1. The validity of these assumptions and performance of the control models in MPC will be tested in this thesis.

3 Theory

In this chapter, the linearised process model used in toolpath optimization of incremental sheet forming is presented. The process can be linearised in multiple ways and the control model that describes the effect of control actions on the product state can be determined using a few different strategies. In section 3.1 the chosen linearisation will be presented and in section 3.2 an overview of the ways in which the control model can be determined will be given.

3.1 Process model

The following section describes the mathematical formulation of the process model and indicates where the uncertainty in the process model is. At t=0, the flat workpiece is located in the xy-plane at z=0. The projection of the space occupied by the product on the xy-plane is denoted as $\boldsymbol{\Omega} \in \mathrm{R}^2$. A number of sampling points on this space is taken and stored in $\boldsymbol{x} \in \boldsymbol{\Omega} \in \mathrm{R}^2$. The considered state of the product $z(\boldsymbol{x}, t)$ is the deflection of the workpiece in z-direction and therefore a scalar function. The change in considered state $\dot{z}(\boldsymbol{x}, t)$ is a function of the complete state of the product (stresses, strains, etc.) $\boldsymbol{Z}(\boldsymbol{\Omega}, t)$ and scalar control action $u(t)$ at time t. Disturbances affecting the state are indicated by $d(\boldsymbol{x}, t)$:

$$\dot{z}(\boldsymbol{x}, t) = f(\boldsymbol{Z}(\boldsymbol{\Omega}, t), u(t), \boldsymbol{x}) + d(\boldsymbol{x}, t) \tag{3.1}$$

The state at time t can be determined by integrating $\dot{z}$ from time 0 to time t:

$$z(\boldsymbol{x}, t) = z(\boldsymbol{x}, 0) + \int_0^t \left[f(\boldsymbol{Z}(\boldsymbol{\Omega}), u(t), \boldsymbol{x}) + d(\boldsymbol{x}, t)\right] dt \tag{3.2}$$

The complexity of the process model is reduced by only including the considered state $z(\boldsymbol{x}, t)$ (deflection) in the process model, instead of complete state $\boldsymbol{Z}(\boldsymbol{\Omega}, t)$. Note that a process model $\tilde{f}$ is always an approximation or simplification of eq. (3.1) and therefore includes model uncertainty $\Delta^f(\boldsymbol{x}, t)$:

$$\dot{z}(\boldsymbol{x}, t) = \tilde{f}(z(\boldsymbol{x}, t), u(t), \boldsymbol{x}) + \Delta^f(\boldsymbol{x}, t) + d(\boldsymbol{x}, t) \tag{3.3}$$

The mathematical description of the process in eq. (3.3) is non-linear. For ISF it is not yet possible to create a model that is sufficiently fast to use in closed-loop control, without reducing model complexity. Therefore the process is linearised around a reference toolpath of which the state over time is known. This process will from now on be referred to as the nominal process. For a nominal path $\bar{u}(t)$, the state evolution $\bar{z}(\boldsymbol{x}, t)$ can be measured in experiments or estimated using a Finite Element model. If the control system is linearised around this nominal process, it is assumed that corrections $\Delta u(t)$ on the nominal path $\bar{u}(t)$ have a linear effect on the state $z(\boldsymbol{x}, t)$. First, the system is discretized. Time is discretized to $t_k, \{k = 1, 2, ...N_t\}$ and space to $x^i, \{i = 1, 2, ...N_x\}$, i.e. for $f_k^i(z_k(\boldsymbol{x}), u_k)$, superscript i indicates the spatial discretization and subscript k indicates the time discretization. The change in state $\dot{z}(\boldsymbol{x}, t) = f(z(\boldsymbol{x}, t), u(t), \boldsymbol{x}, t)$ can now be linearised around the nominal toolpath using a Taylor expansion:

$$f_k^i(z_k(\boldsymbol{x}), u_k) = f_k^i(\bar{z}_k(\boldsymbol{x}), \bar{u}_k) + \sum_j \left.\frac{\partial f_k^i}{\partial z_k^j}\right|_{\bar{\boldsymbol{z}}_k, \bar{u}_k} (z_k^j - \bar{z}_k^j) + \left.\frac{\partial f_k^i}{\partial u_k}\right|_{\bar{\boldsymbol{z}}_k, \bar{u}_k} (u_k - \bar{u}_k) + \text{H.O.T.} \tag{3.4}$$

In its most general form, the state of all spatial discretization points have an influence on the change of state in a single spatial discretization point, hence the sum in the second term. Defining

$\Delta z_k^j = z_k^j - \bar{z}_k^j$ and $\Delta u_k = u_k - \bar{u}_k$ and omitting higher order terms gives:

$$\dot{z}_k^i \approx f_k^i(\bar{z}_k(\boldsymbol{x}), \bar{u}_k) + \sum_j \left.\frac{\partial f_k^i}{\partial z_k^j}\right|_{\bar{\boldsymbol{z}}_k, \bar{u}_k} \Delta z_k^j + \left.\frac{\partial f_k^i}{\partial u_k}\right|_{\bar{\boldsymbol{z}}_k, \bar{u}_k} \Delta u_k \tag{3.5}$$

For notational simplicity, from now on we store all spatially discretized elements in bold vectors (i.e. $z^i \in \boldsymbol{z}$). The gradients of f will be stored in time-varying matrix $\boldsymbol{\mathcal{A}}_k$ and vector $\boldsymbol{\mathcal{B}}_k$

$$\dot{\boldsymbol{z}}_k \approx \boldsymbol{f}_k(\bar{z}_k(\boldsymbol{x}), \bar{u}_k, \boldsymbol{x}) + \boldsymbol{\mathcal{A}}_k \Delta \boldsymbol{z}_k + \boldsymbol{\mathcal{B}}_k \Delta u_k \tag{3.6}$$

With $\boldsymbol{\mathcal{A}}_k$ and $\boldsymbol{\mathcal{B}}_k$ being:

$$\boldsymbol{\mathcal{A}}_k = \left.\frac{\partial \boldsymbol{f}_k}{\partial \boldsymbol{z}_k}\right|_{\bar{\boldsymbol{z}}_k, \bar{u}_k} \qquad \boldsymbol{\mathcal{B}}_k = \left.\frac{\partial \boldsymbol{f}_k}{\partial u_k}\right|_{\bar{\boldsymbol{z}}_k, \bar{u}_k} \tag{3.7}$$

The state evolution can be predicted by:

$$\boldsymbol{z}_{k+1} \approx \boldsymbol{z}_k + \Delta t_k \dot{\boldsymbol{z}}_k \tag{3.8}$$

With $\Delta t_k = t_{k+1} - t_k$ and nominal state evolution $\Delta t_k \boldsymbol{f}_k(\bar{z}_k(\boldsymbol{x}), \bar{u}_k) = \bar{\boldsymbol{z}}_{k+1} - \bar{\boldsymbol{z}}_k$:

$$\boldsymbol{z}_{k+1} \approx \boldsymbol{z}_k + \bar{\boldsymbol{z}}_{k+1} - \bar{\boldsymbol{z}}_k + \Delta t_k \left(\boldsymbol{\mathcal{A}}_k \Delta \boldsymbol{z}_k + \boldsymbol{\mathcal{B}}_k \Delta u_k\right) \tag{3.9}$$

When it is assumed that there is no dependency of the state evolution on small deviations from the nominal state, $\boldsymbol{\mathcal{A}}_k = 0$. The final geometry $\boldsymbol{z}_{N_t}$ after the last step of the process can be predicted by:

$$\boldsymbol{z}_{N_t} \approx \boldsymbol{z}_k + \bar{\boldsymbol{z}}_{N_t} - \bar{\boldsymbol{z}}_k + \sum_{j=k}^{N_t-1} \Delta t_j \boldsymbol{\mathcal{B}}_j \Delta u_j \tag{3.10}$$

When the linearisation is evaluated at time step k, only the corrections Δu in the future will be included. These corrections are stored in $\Delta \boldsymbol{u}_k$, which is a truncation of the complete series of control actions in the process $\Delta \boldsymbol{u}$:

$$\Delta \boldsymbol{u}_k = [\Delta u_k, \Delta u_{k+1}, \ldots, \Delta u_{N_t-1}]^T \tag{3.11}$$

The effect of the control actions $\Delta t_k \boldsymbol{\mathcal{B}}_k$ will be stored in columns $\boldsymbol{g}_k$ of matrix $\boldsymbol{G}_k$. Consistent with $\Delta \boldsymbol{u}_k$, $\boldsymbol{G}_k$ is a truncation of complete matrix $\boldsymbol{G}$, corresponding to the future control actions only.

$$\boldsymbol{G}_k = [\boldsymbol{g}_k, \boldsymbol{g}_{k+1}, \ldots, \boldsymbol{g}_{N_t-1}] \tag{3.12}$$

With these definitions, the linearisation can conveniently be written in matrix-vector notation:

$$\boldsymbol{z}_{N_t} \approx \boldsymbol{z}_k + \bar{\boldsymbol{z}}_{N_t} - \bar{\boldsymbol{z}}_k + \boldsymbol{G}_k \Delta \boldsymbol{u}_k \tag{3.13}$$

In other words, the final state can be predicted by the adding the nominal state evolution and effect of future corrections $\Delta \boldsymbol{u}_k$ to the current state. The columns in $\boldsymbol{G}_k$ describe the effect of the corrections in $\Delta \boldsymbol{u}_k$ and the nominal state evolution $\bar{\boldsymbol{z}}_{N_t} - \bar{\boldsymbol{z}}_k$ describes the evolution of the process when no control would be applied. This linear system can now conveniently be used in a controller.

3.2 Control model definitions

The control model $\boldsymbol{G}$ that describes the effect of control actions $\Delta \boldsymbol{u}$ on the final geometry can be chosen in many different ways. The most commonly used model is the impulse response approach as described in section 2.3.2. The model contains the state evolution of the nominal process, normalized by step height u_k. Each impulse response describes the change of the shape of the product between step k and step $k+1$. It is assumed that the effect of a correction on the step height Δu is equal to this nominal state evolution.

Definition 1 - Full nominal step $$\boldsymbol{g}_k = \frac{\bar{\boldsymbol{z}}_{k+1} - \bar{\boldsymbol{z}}_k}{\bar{u}_k} \tag{3.14}$$

This definition only requires information on the nominal state evolution, which can be determined using either experiments or Finite Element Analysis.

In definition 1, there is an assumption that a control action Δu_k has the same effect on the process as nominal step $\bar{u}_k$. A more exact control model can be constructed by comparing the nominal process with a process in which a control action is applied. This will be the basis of control model definitions 2, 3 and 4. The state of a process in which a single control action Δu is applied at step k will be named $\boldsymbol{z}_k(\Delta u_k)$. At all other steps than the corrected step, the nominal step height is used. Note that this still implies that all contours after the corrected step will move. In definition 2, the control model is constructed by comparing the state at step $k+1$, right after the control action is applied at step k.

Definition 2 - Response at step $k+1$ $$\boldsymbol{g}_k(\Delta u_k) = \frac{\boldsymbol{z}_{k+1}(\Delta u_k) - \bar{\boldsymbol{z}}_{k+1}}{\Delta u_k} \tag{3.15}$$

In experiments this would require at least one extra test per step k and preferably more to ensure validity. In Finite Element Analysis, the analysis of the nominal process can be restarted at every time instance using different parameters and toolpath.

If definition 2 is used in a linearisation to predict the final state of the process, the linearisation involves the assumption that the influence of Δu_k on $\boldsymbol{z}_{k+1}$ is the same as its influence on $\boldsymbol{z}_{N_t}$. It will however be shown that this is not the case, and therefore a different response can be found when determining the effect of Δu_k on the final state of the product. This control model is named definition 3:

Definition 3 - Response at step N_t $$\boldsymbol{g}_k(\Delta u_k) = \frac{\boldsymbol{z}_{N_t}(\Delta u_k) - \bar{\boldsymbol{z}}_{N_t}}{\Delta u_k} \tag{3.16}$$

Note that although possibly more accurate, it is computationally very expensive to determine definition 3. Where definition 2 requires one additional analysis step per time step ($N_t - 1$ steps), definition 3 requires an additional $(N_t - 1) - (k - 1)$ analysis steps for an analysis of Δu_k, which results in approximately $\frac{1}{2}(N_t - 1)^2$ steps.

When a control action Δu_k at step k has a different effect on the state of step $k+1$ than on the state of step N_t, it can be assumed that it has a different effect on every step in between. This also implies that a control action in the past can still have an effect on the state evolution in the future and thus should be included in the linearisation. In definition 4, the linearisation contains an additional term taking into account the influence of control actions in the past:

Definition 4 - History aware $$\tilde{\boldsymbol{z}}_{N_t} = \boldsymbol{z}_k + \bar{\boldsymbol{z}}_{N_t} - \bar{\boldsymbol{z}}_k + \boldsymbol{Q}_{his,k} \Delta \boldsymbol{u}_{his,k} + \boldsymbol{Q}_{opt,k} \Delta \boldsymbol{u}_{opt,k} \tag{3.17}$$

For use in an optimization algorithm, the optimization variables $\Delta \boldsymbol{u}_{opt,k}$ should be split from the effect of control steps which are already performed $\Delta \boldsymbol{u}_{his,k}$:

$$\Delta \boldsymbol{u}_{his,k} = [\Delta u_1, \Delta u_2, \ldots, \Delta u_{k-1}]^T \tag{3.18}$$

$$\Delta \boldsymbol{u}_{opt,k} = [\Delta u_k, \Delta u_{k+1}, \ldots, \Delta u_{N_t-1}]^T \tag{3.19}$$

In the same fashion, $\boldsymbol{Q}_{his,k}$ and $\boldsymbol{Q}_{opt,k}$ are the corresponding matrices that contain the effect of the control actions on the final geometry. How these matrices are filled can be read in appendix B.1. The term that accounts for historic actions could be seen as a correction on the nominal state evolution at each MPC run.

The computational costs or experimental efforts of the definitions above make a simplification attractive. For simple products, the cumulative Weibull function makes a good fit to most of the models above. The cumulative Weibull function has been used as a model by Wang et al. [24] and Allwood et al. [23] before, as described in section 2.3.2. The Weibull function is a function of the radial coordinate, with an offset r_0, shape parameters λ and k and scaling h:

Definition 5 - Weibull fit
$$W^i = \begin{cases} he^{(-\frac{r^i - r_0}{\lambda})^k}, & \text{if } r^i \geq r_0 \\ h, & \text{otherwise} \end{cases} \tag{3.20}$$

In the following chapters, the validity of the assumptions in section 2.3.1 will be investigated and the models defined above will be presented. These models will be used in a controller and tested on Finite Element simulations of the process.

4 | Axisymmetric products

The products in this chapter are axisymmetric geometries created by a series of circular z-level contours. These products are simple and insightful and therefore suitable for an in-depth analysis of the control theory presented in chapter 3. The definition of the toolpath and control problem will be given in section 4.1. The nominal process on which the control system will be applied will be explained in section 4.2. An analysis of the impulse response will be done in section 4.3. In section 4.4, the MPC will be tested on its accuracy, stability, robustness and its applicability on closely related target geometries. In Chapter 5 the knowledge gained in this chapter will be used to do research on more complex products.

4.1 Methodology

Each time step k in the process contains 1 circular z-level contour, described by a radial and height coordinate (r_k,z_k). The step height between contour $k-1$ and contour k is defined as u_k:

$$u_k = \mathrm{z}_k - \mathrm{z}_{k-1} \tag{4.1}$$

Where z_k is the z-coordinate of contour k. Figure 4.2 shows these definitions schematically. The initial state of the process is $\boldsymbol{z}_1$. Because of this, each contour k has a state $\boldsymbol{z}_{k+1}$ as a result. The state is the deflection perpendicular to the initially flat sheet, which can also be seen as the height of the product if the undeformed sheet is placed at z = 0 mm.. The tool is retracted from the product after every contour to measure the deflection after springback. With N_t time steps, there are $N_t - 1$ contours and corresponding step heights u_k. The state z_k is reduced to a two-dimensional problem by using the axial symmetry. A number of radial samples is averaged over the circumference. A more detailed explanation of this sampling can be found in appendix C. Figure 4.1 gives an example of the target geometry of an axisymmetric product made using circular z-level contours.

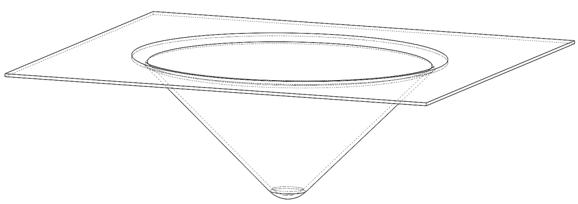

Figure 4.1: 45^o cone geometry

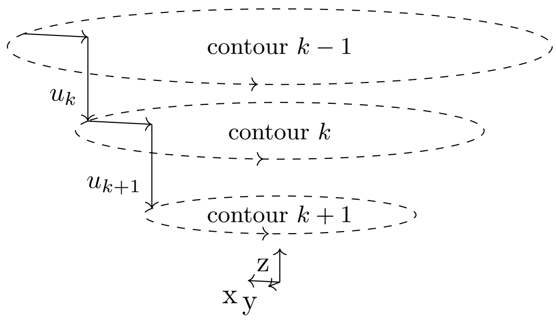

Figure 4.2: Path definition

When using control, corrections Δu_k will be made on nominal step height $\bar{u}_k$. Note that this has as a result that when a correction on the step height is applied at step k, all contours from step k to step N_t will move. The nominal path is defined by a fixed $\bar{u}_k$ for every step, after which the radial coordinates r_k are calculated using the contour-following method. This method calculates where the center of the tool should be to touch the target geometry tangentially.

4.2 Nominal analysis

A cone with a constant wall-angle of 45^o will be used as a test product in this chapter. The size of the sheet is 150x150 mm and the sheet is clamped around its edges. The nominal step height between the contours is $\bar{u}$ = -1 mm and the tool radius is 7.5 mm. The target geometry is shown in fig. 4.3. The resulting mean height over the circumference when following the nominal path is plotted in fig. 4.5. Figure 4.6 shows the impulse response determined with *Def. 1 - Full nom. step* in section 3.2, which can be constructed with data from the nominal process alone.

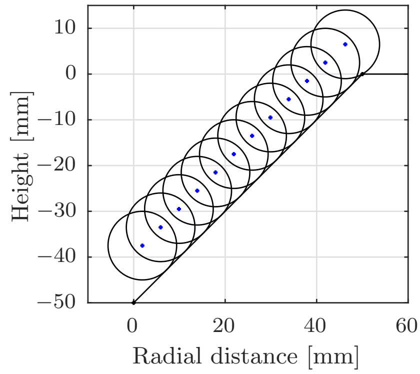

Figure 4.3: Straight 45^o cone target geometry. The circles represent a part of the tool locations.

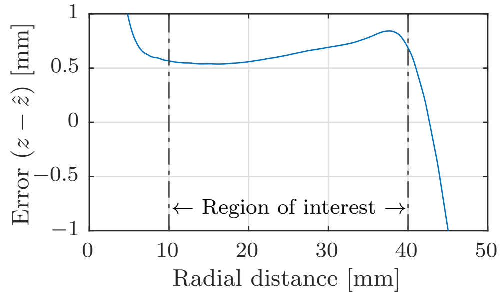

Figure 4.4: Mean error over the circumference.

As the tool moves radially inwards, the impulse response plot should be read from right to left, as the gradient of colors indicates. The responses of the first few steps are very wide and lower than 1 because of global bending and elastic springback. The peaks of the impulse responses above 1 and below 0 are the result of the indentation of the tool. The magnification in fig. 4.5 shows that the final geometry is slightly less deep than the target. The error is defined as the actual final geometry minus the target geometry and shown in fig. 4.4. A negative error indicates that the actual geometry is too deep or ”overformed”, where a positive error indicates that the actual geometry is not deep enough or ”underformed”.

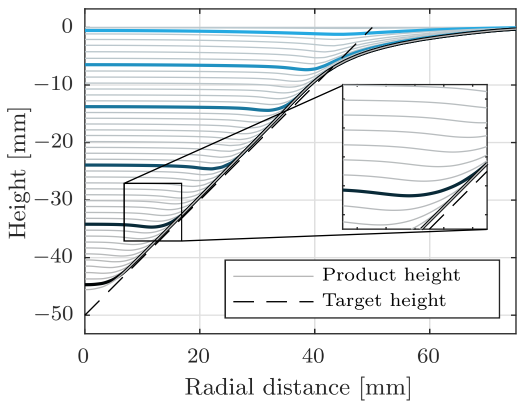

Figure 4.5: Height $\boldsymbol{z}_{k+1}$ after each step k.

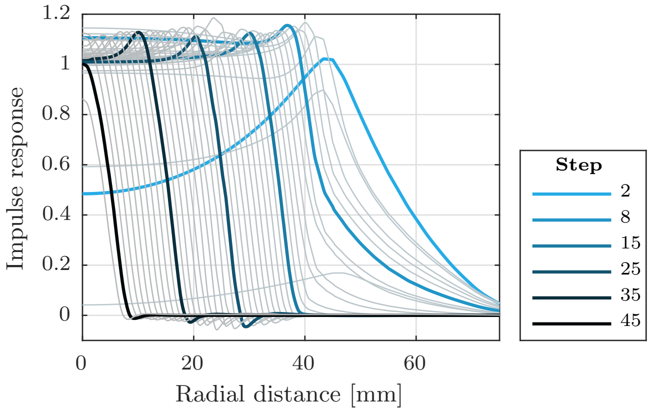

Figure 4.6: Impulse response $\boldsymbol{g}_k$ of each step according to *Def. 1 - Full nom. step* in section 3.2.

The spatial discretization points are located in the region of interest ($10 \leq r \leq 40$ mm), as indicated in fig. 4.4, to exclude areas which contain an error that can not be reduced much with any toolpath correction. The Euclidean norm of the error (eq. (4.3)) at the discretization points is 8.03 when following the nominal toolpath. This is used as a reference throughout this chapter.

4.3 Impulse response analysis

To use impulse responses as a control model in MPC, they should be sufficiently linear with the control action and the effect should be instantaneous (time-consistent). The extent to which these assumptions hold for the definitions in section 3.2 will be evaluated in this section. The assumption of spatially invariance is necessary to reduce the axisymmetric product to a 2D problem, where state and response are only a function of the radius, but is of less significance for the working of the MPC after making that simplification. For an analysis of the spatial invariance of axisymmetric products, the reader is referred to appendix C.

4.3.1 Linearity

Since the impulse response is normalized by the correction Δu_k, the impulse response should be similar for every magnitude of the control action within reasonable range. As described in section 3.2, control models can be determined by restarting a Finite Element Analysis with a different toolpath and comparing to the nominal analysis. Below, the impulse response models according to *Def. 2 - Resp. at* $k+1$ and *Def. 3 - Resp. at* N_t are determined using different values of Δu_k between -1 and 1 mm. Since the nominal value $\bar{u}_k$ = -1 mm, it does not make sense to make corrections larger than 1 mm. Note that a negative Δu_k represents a larger and thus deeper step, where a positive Δu_k represents a smaller and thus less deep step.

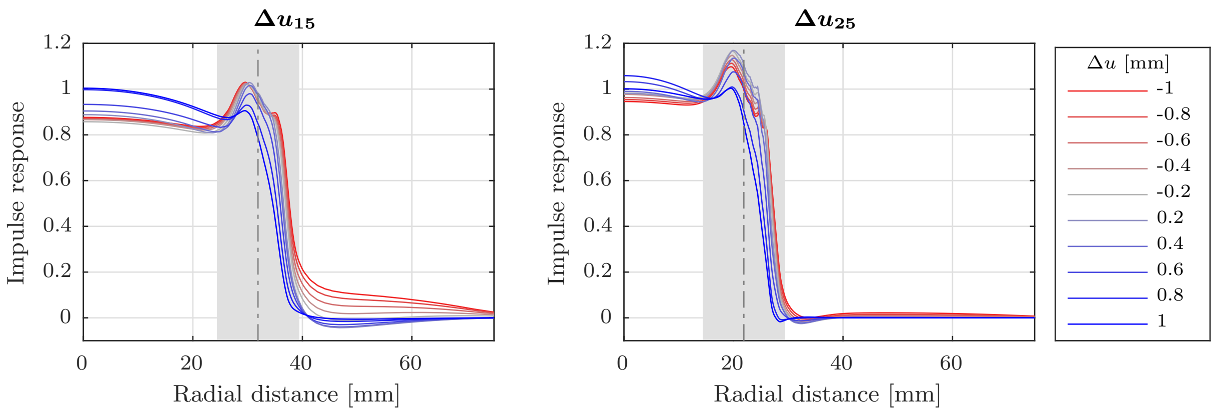

Figure 4.7: Linearity of *Def. 2 - Resp. at* $k+1$ at step 15 and step 25. The gray area illustrates the location of the tool

Figure 4.7 shows the impulse response according to *Def. 2 - Resp. at* $k+1$ for different magnitudes of Δu_k when applied at step 15 and at step 25. A non-linearity present in both graphs is the variance at the inside of the product (low radii). This represents the pillow effect. This non-linearity is significant, but not very alarming since it is located in a region where the tool will also have an effect in future steps. Therefore the inaccuracies caused by the pillow effect should be accounted for by the MPC.

More important is the non-linearity in the region with a response close to 0 in the analysis of step 15. For negative Δu_{15}, the impulse response is bigger than zero, indicating global bending of the product. If a negative Δu is applied, it is desired that this feature is present in the impulse response, but if this impulse response determined with negative Δu is used as a model and a positive Δu is applied, the impulse response model predicts that the product can actually be formed back upwards in that region. This obviously does not happen and can result in an inaccurate control system.

Figure 4.8 shows the linearity of the impulse response according to *Def. 3 - Resp. at N_t* . The non-linearity in step 15 due to global bending is present in this case, but a change in the pillow effect can not be observed. Another important non-linearity is observed in the region where the response increases from a value of 0 to a value of 1. The impulse response shifts radially inwards with positive Δu_k and radially outwards with negative Δu_k. This feature can also be seen in fig. 4.7. Similar to the non-linearity originating from global bending, this feature can also make wrong predictions in a region where the tool will not be able to correct any mistakes.

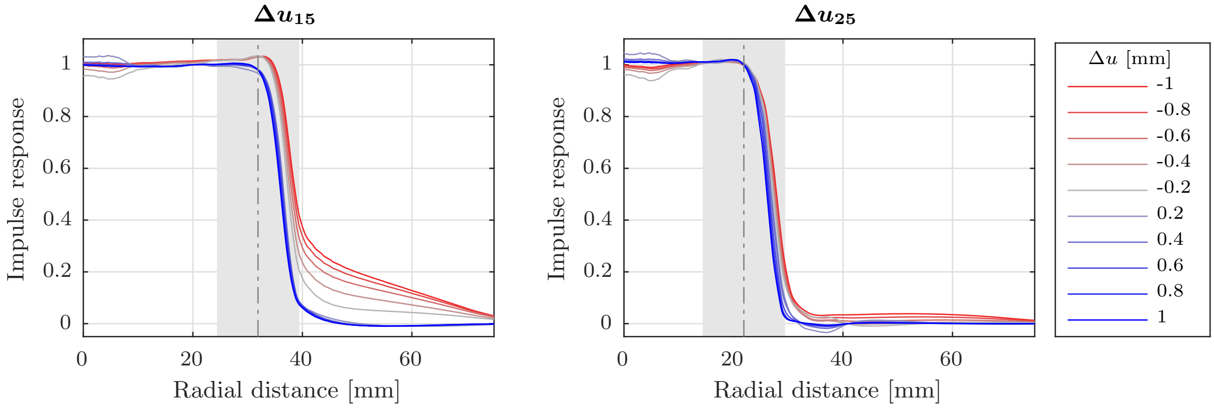

Figure 4.8: Linearity of *Def. 3 - Resp. at N_t* at step 15 and step 25. The gray area illustrates the location of the tool

4.3.2 Time-consistency

The linearisation in the MPC relies on the assumption that a control action at step k has the same effect on the geometry at step $k+1$ as on the geometry at step N_t. The difference between the response at step $k+1$ and the response at step N_t in the previous section proves that this is not the case. The response changes in between those steps. This indicates that a control action in the past can still have an effect on the state of future steps and should thus be included in the prediction in the MPC. Normally only the effect of control actions from current step k to final step $N_t - 1$ are included in the linearisation. By comparing an analysis in which a control action is applied ($\boldsymbol{z}_l(\Delta u_k)$) with the nominal analysis ($\bar{\boldsymbol{z}}_l$) at every step l, this effect can be investigated. For control step Δu_k, the difference between state $\boldsymbol{z}_{l+1}(\Delta u_k)$ and nominal state $\bar{\boldsymbol{z}}_{l+1}$ is stored in $\boldsymbol{r}_l$, which is a column of matrix $\boldsymbol{R}_k$ corresponding to a correction at step k:

$$\boldsymbol{r}_l = \frac{\boldsymbol{z}_{l+1}(\Delta u_k) - \bar{\boldsymbol{z}}_{l+1}}{\Delta u_k} \tag{4.2}$$

When l = k, *Def. 2 - Resp. at $k+1$* is described and when l = $N_t - 1$, *Def. 3 - Resp. at N_t* is described. Figure 4.9 shows the evolution of the impulse response from $l = k$ to $l = N_t - 1$ with the responses of steps in between in gray. It can be seen that for step 1 and 5, early in the process, the responses changes significantly over time at the whole product. For later steps, the difference is mainly in the pillow, which is the region around a response of 1.

The results show that the moment at which the response is evaluated is important. While *Def. 1 - Full nom. step* and *Def. 2 - Resp. at $k+1$* are computationally less expensive than *Def. 3 - Resp. at N_t* , choosing for the last makes the most sense since the control system optimizes for the final geometry. As explained in section 3.2, the fact that the response changes over time indicates that the effect of a control action is not instantaneous. This means that control actions in the past should also be included in the linearisation when predicting the final geometry, which can be done using the information gathered in this analysis of the response over time. The mathematical description of the terms that describe this effect in *Def. 4 - History aware* can be found in appendix B.1.

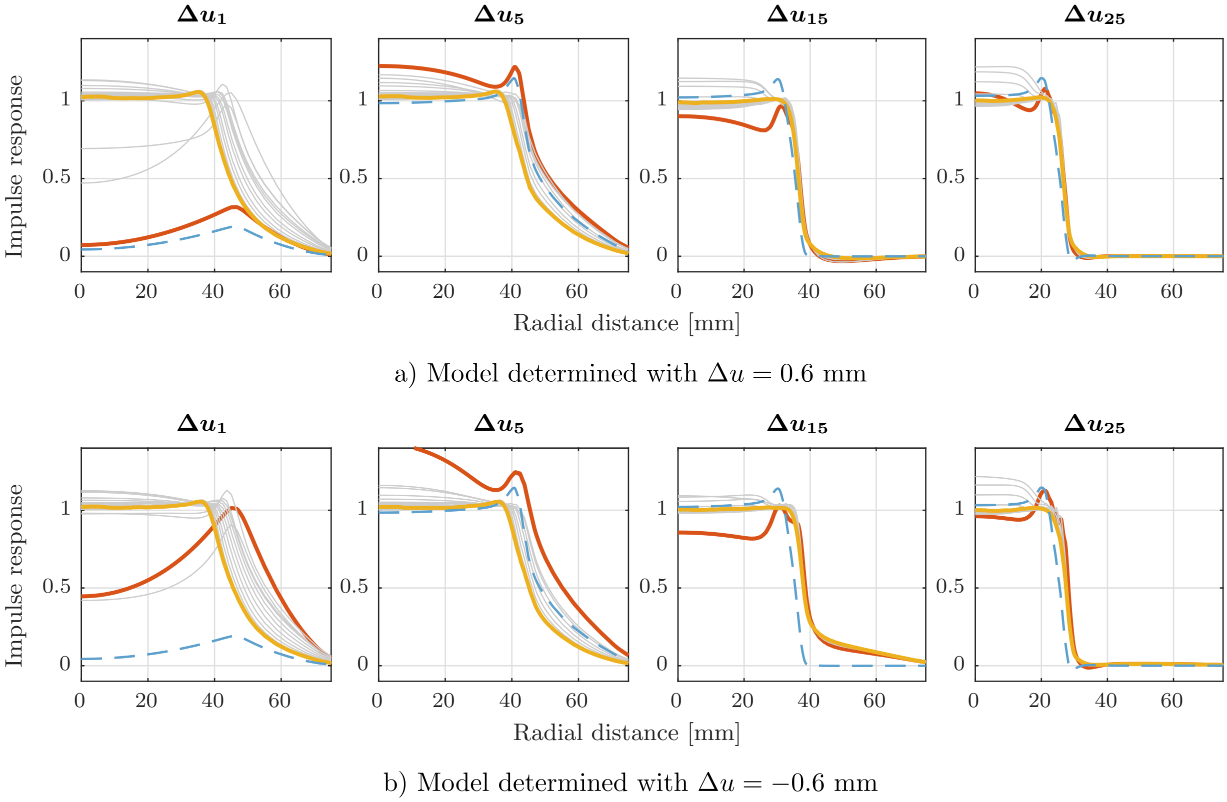

Figure 4.9: Evolution of the impulse response determined with $\Delta u = \pm 0.6$ mm from step k (— Def. 2) to step $N_t - 1$ (— Def. 3). The responses between those steps can be seen in gray. As a reference, *Def. 1 - Full nom. step* is included as the dashed line (- -).

4.3.3 Models

The control models that will be used to test the MPC performance will be determined by applying a single correction on the step height $\Delta u_k = \pm 0.6$ mm at step k, after which the nominal step height $\bar{u} = -1$ mm is used in the other steps. This means that to construct the models in the following figures, a separate finite element analysis has to be run for each response line. Figure 4.10 gives the results of determining the impulse response model using *Def. 2 - Resp. at $k+1$* and Figure 4.11 gives the results of determining the impulse response model using *Def. 3 - Resp. at N_t*. The models are determined using $\Delta u = 0.6$ mm and $\Delta u = -0.6$ mm because the controller will be bounderd by $-0.5 \leq \Delta \leq 0.5$ mm and the linearity analysis in section 4.3.1 is done in steps of 0.2 mm.

Some notable differences between the two definitions and the two directions of the correction can be observed. In *Def. 2 - Resp. at $k+1$*, the impulses are similar to *Def. 1 - Full nom. step* (fig. 4.6). The peaks that are observed correspond to the indentation of the tool and the high response at the first steps in the center of the cup (in between 1 and 1.5) is caused by bulging of the center of the cup, which is named the pillow-effect.

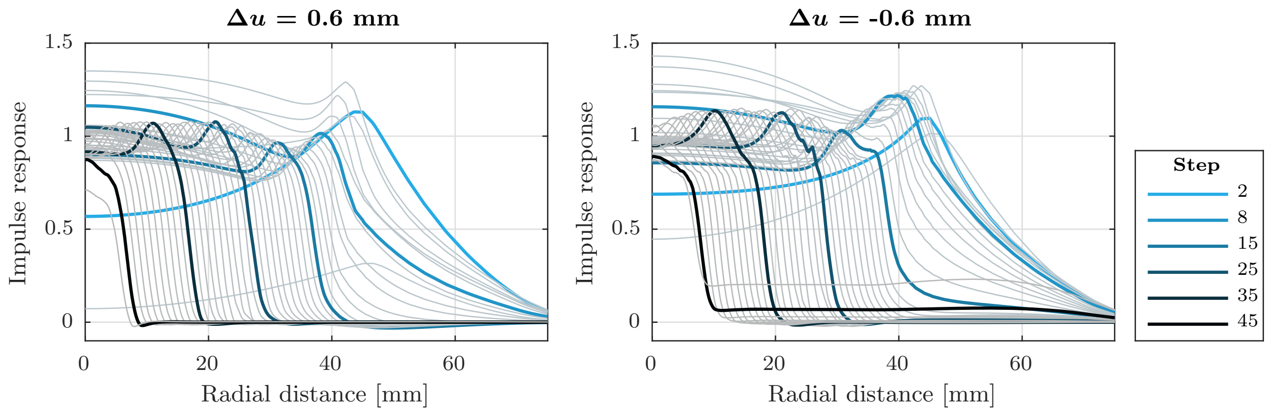

Figure 4.10: Impulse response determined using *Def. 2 - Resp. at* $k+1$

In *Def. 3 - Resp. at* N_t , these features are not present. The impulse response of most steps is very close to zero radially outward from the tool,very close to one inwards from the tool and gradually increases in between. This is much like the proposed *Def. 5 - Weibull fit* model. The difference between *Def. 2 - Resp. at* $k+1$ and *Def. 3 - Resp. at* N_t indicates that the effect of a control actions is not instantaneous and will change over future time steps. As the MPC aims to minimize the different between the final geometry and the target, it is expected that *Def. 3 - Resp. at* N_t will perform best.

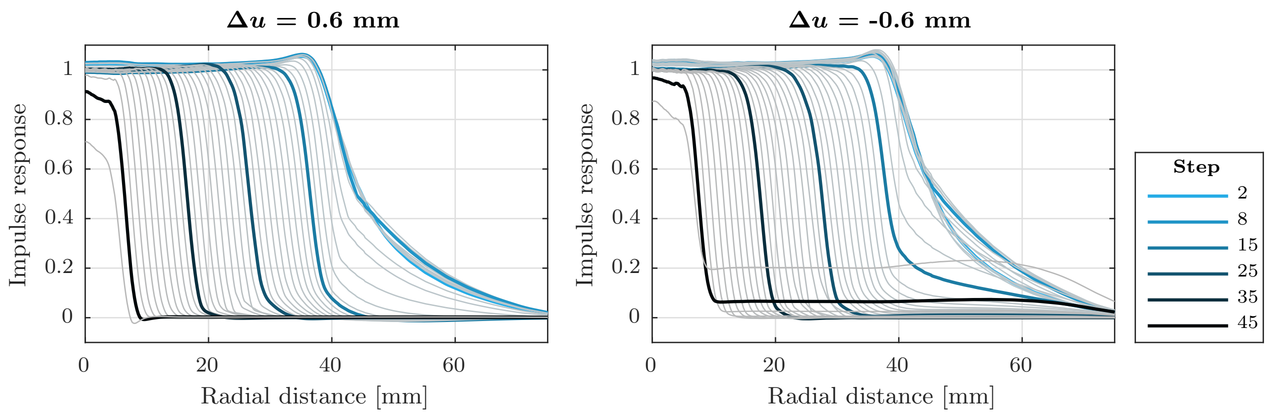

Figure 4.11: Impulse response determined using *Def. 3 - Resp. at* N_t

4.3.4 Large deviations from the nominal path

When the linearity of the impulse response was evaluated in section 4.3.1, the control actions were applied at a single step, before and after which the nominal step size was used. This does not give any information on the influence of one control action on another. In this section, the validity of the impulse response and state evolution after deviating from the nominal toolpath at multiple steps is evaluated.

In the following analyses, a correction of 0.15 mm during the first 15 steps is applied with respect to the nominal toolpath ($\Delta u_i = \pm 0.15 \quad \forall i \in \{1, 2, \ldots, 15\}$) after which the nominal path with the nominal step height $\bar{u} = -1$ mm is followed. This is done for both negative corrections (deeper) and positive directions (less deep) in separate analyses. The state evolution after this step ($\boldsymbol{z}_{N_t} - \boldsymbol{z}_{16}$) is assumed be equal to the nominal state evolution ($\bar{\boldsymbol{z}}_{N_t} - \bar{\boldsymbol{z}}_{16}$). In this analysis, a difference was observed. In fig. 4.12, the nominal state evolution after step 16 is subtracted from the actual state evolution and plotted as a solid line. In section 4.3.2, it was illustrated that the control actions from step 1 to 15 can still have an effect from step 16 to N_t.

If this effect is predicted by the corresponding term in *Def. 4 - History aware* ($\boldsymbol{Q}_{his,16}\boldsymbol{\Delta u}_{his,16}$), the dashed lines in fig. 4.12 are the result. This shows that *Def. 4 - History aware* can capture some of the change in state evolution due to control actions in the past and can thus be seen as a correction on the nominal state evolution.

Next to the state evolution, the validity of the impulse response model is also questionable at large deviations from the nominal path. Therefore, analyses were done where an additional control action of ± 0.5 mm is applied at step 16 ($\Delta u_{16} = \pm 0.5$ mm) after the corrections at step 1 to 15. These were compared to the analyses of the state evolution in which only step 1 to 15 were corrected. The impulse response can be constructed by *Def. 3 - Resp. at N_t* and be compared with the impulse response models determined at the nominal toolpath, as shown in section 4.3.3. Figure 4.13 shows this comparison with the solid lines being the impulse response when deviated from the nominal toolpath and the dashed lines being the response at the nominal toolpath.

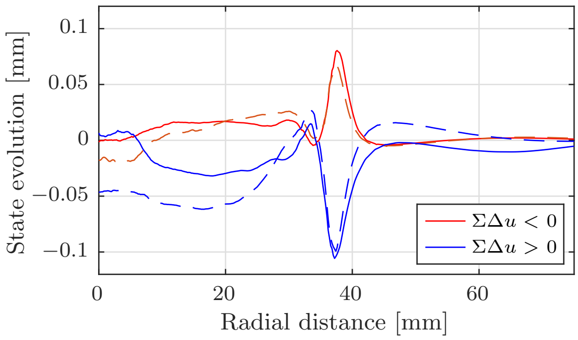

Figure 4.12: Change from nominal state evolution after deviating from the nominal path. The solid line indicates the actual deviation and the dashed line indicates the prediction of this deviation by *Def. 4 - History aware*

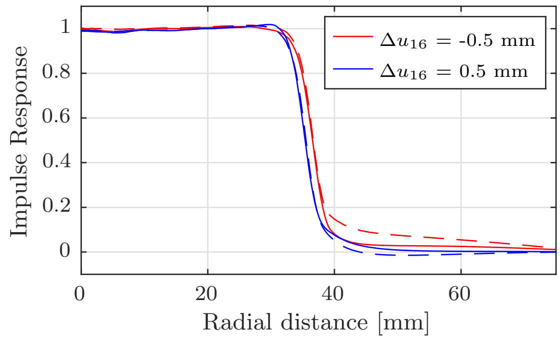

Figure 4.13: Impulse response of step 16 determined with *Def. 3 - Resp. at N_t* after applying a control action when deviated from the toolpath. The dashed line is the impulse response at the nominal path.

It can be noted that at the outside of the product (high radii), the impulse response is not equal to the impulse response at the nominal path, which can be problematic since this is a region that will not be visited by the tool after the evaluated step. This result means that not only the nominal state evolution is affected by deviations from the toolpath, but also the impulse response is dependent on the control history. For the nominal state evolution this effect can be captured by *Def. 4 - History aware* . For the impulse response, such an approach is not available.

4.4 MPC Performance

The main objective of the models that have been discussed before, is to allow for accurate closed-loop process control. In the following section, the performance of the developed linearisation and control models will be tested in a numerical environment. The process model is used to optimize the step height between the z-level contours in the toolpath by means of Model Predictive Control, as explained in section 2.2.2.

The closed-loop performance will be compared with open-loop performance and the robustness of the controller against parameter variation will be tested. The last sections will evaluate the performance of the controller when the target geometry is different than the target geometry of the process that the model is linearised around. A few different approaches for this case will be given.

4.4.1 Methodology

In this work, a simple target geometry with sharp wall angle transitions is used, as shown in fig. 4.3. The tip of the cone in the bottom of the product is a feature which is impossible to form due to the radius of the tool and the lack of support of dies makes that global bending near the clamping is inevitable. If the regions in which these sources of error are present are included in the optimization problem, the MPC will try to reduce these large errors at the expense of smaller errors which can be reduced rather easily. Therefore these regions are excluded and only the spatial discretization points in the region of interest ($10 \leq r \leq 40$ mm) will be used. This reduces the size of the state vector that is considered, but also reduces the size of the impulse response matrix.

The performance of the MPC can be seen best when looking at the resulting error plot and error norms. These results will be presented side by side in the following sections. The error norms are Euclidean error norms and calculated by:

$$\|e\| = \sqrt{\sum_{i=1}^{N_x} (e^i)^2} \tag{4.3}$$

Where e^i is the error at sampling point i, defined by $e^i = z^i - \hat{z}^i$.

In the following sections, the error norms as a result of applying Model Predictive Control will be given in tables. The black value in the table indicates the actual error norm after running the MPC in closed-loop. The grey value between brackets indicates the theoretical minimum. The theoretical minimum is the minimum value of the error norm as a result of the optimal path as predicted by the MPC in open-loop. In other words, it is the best that the MPC thinks it can do. The difference between this theoretical minimum and the actual error gives an indication of the model error, the accuracy of the used linearisation.

Impulse response definitions 2, 3, 4 and 5 are determined by running a finite element analysis with a correction Δu. Constructing the models using a positive or negative Δu as a correction results in different models. Only a single model can be used in the linearisation developed. The MPC performance will be evaluated for both directions of corrections when determining the control models.

The applied control actions for all models and directions of control will not be given in this chapter, but can be found in appendix E.1 Unless mentioned otherwise, the MPC is run with weight factor $\alpha = 2$ and bounds $-0.5 \leq \Delta u \leq 0.5$ mm as defined in eq. (2.1).

4.4.2 Open-loop

An MPC is most effective when used in closed-loop with the use of state feedback. The state feedback accounts for model error, disturbances and measurement error. The MPC can also be used in open-loop, where it only solves the optimization problem at k=1, before the start of the process. The complete optimized control strategy is then applied to the nominal toolpath and executed. The performance of this toolpath gives insight in the accuracy of the control model. In a practical application an open-loop approach can be favourable because it does not require the use of state sensors, which reduces process time and complexity.

Figure 4.14 shows the optimal control strategy as determined by the open-loop MPC. The figure on the left shows the corrections Δu, which is the actual output of the MPC. The figure on the right shows the cumulative value of Δu, which represents how far the new toolpath deviates from the original toolpath. Note that *Def. 4 - History aware* reduces to *Def. 3 - Resp. at N_t* when evaluated at k=1. At k=1, no steps have been performed and $\Delta \boldsymbol{u}_{his}$ is not available yet.

The largest difference in toolpath strategy between the models is seen in the first few steps. Since the tool moves radially inward, the error at the outside of the product corresponds to the strategy in the first steps.

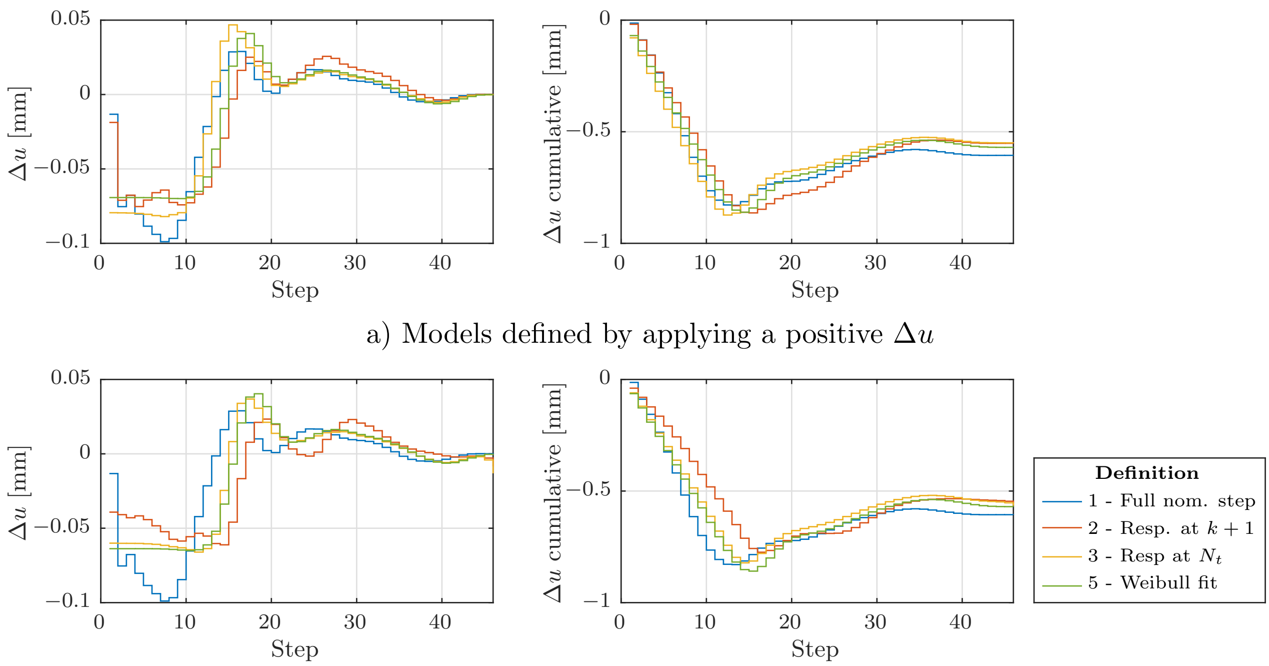

a) Models defined by applying a positive Δu

b) Models defined by applying a negative Δu

Figure 4.14: Optimal control strategy according to an open-loop MPC run

Figure 4.15 shows the resulting error of the open-loop strategy. The strategy proves to be a significant improvement compared to following the nominal toolpath. The commonly used *Def. 1 - Full nom. step* proves to work well, but is still far away from its theoretical minimum compared to other definitions, indicating that there is a significant model error. *Def. 3 - Resp. at N_t* performs very well and close to the theoretical minimum, indicating that the model is more accurate than others. *Def. 5 - Weibull fit* is derived from *Def. 3 - Resp. at N_t* but performs more poorly. *Def. 2 - Resp. at $k+1$* contains a large error at the outside of the product and performs worse than the more straightforward definition 1. The error for models determined with positive Δu and negative Δu is comparable. Note that in this analysis, the models are tested on the same Finite Element analysis as they were constructed with. No disturbances or model error due to unmodelled physics are present here.

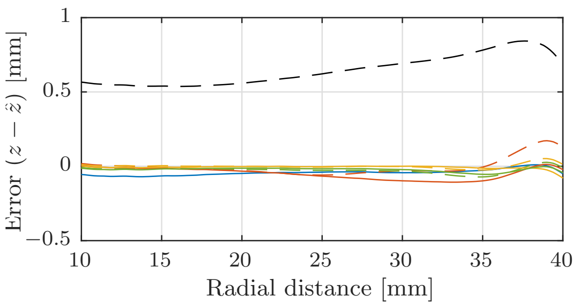

(a) Error from target

Impulse response definition	Assumed control direction: Positive Δu (——)	Assumed control direction: Negative Δu (- - -)
- - No control	8.03	
— 1 - Full nom. step	0.57 (0.12)	
— 2 - Resp. at $k+1$	0.76 (0.13)	0.70 (0.14)
— 3 - Resp. at N_t	0.15 (0.12)	0.18 (0.10)
— 5 - Weibull fit	0.31 (0.12)	0.40 (0.12)

(b) Legend including euclidean error norm [mm]. (Theoretical minimum in gray)

Figure 4.15: Open-loop performance straight cone.

4.4.3 Closed-loop

When the MPC is used in closed-loop, the state is measured after each step and used in the MPC to determine a new optimal toolpath. In closed-loop, the MPC should be able to handle disturbances and model error better than in open-loop. Figure 4.16 shows the results of the closed-loop MPC run for different models. The first thing to note is the error compared to the open-loop runs. The differences between the models are smaller in closed-loop and the models that performed worse in open-loop perform better where the models which performed good in open-loop have a slightly worse performance in closed-loop.

New in this analysis is *Def. 4 - History aware* , which includes a term that accounts for influences from control actions in the past on future state evolution. This can be seen as an extension to *Def. 3 - Resp. at* N_t . The error in the table indicates that this definition performs better than *Def. 3 - Resp. at* N_t . In contrary to the open-loop analysis, the models determined with a positive Δu behave very different from those determined with negative Δu . The models determined with negative Δu appear to initiate some oscillation of the error at the outside of the product. This can be seen for all definitions.

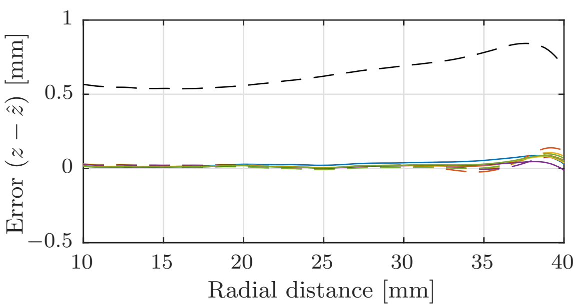

(a) Error from target

Impulse response definition	Assumed control direction: Positive Δu (——)	Assumed control direction: Negative Δu (- - -)
- - No control	8.03	
— 1 - Full nom. step	0.49 (0.12)	
— 2 - Resp. at $k+1$	0.35 (0.13)	0.49 (0.14)
— 3 - Resp. at N_t	0.34 (0.12)	0.41 (0.10)
— 4 - History	0.25 (0.12)	0.31 (0.10)
— 5 - Weibull fit	0.37 (0.12)	0.34 (0.12)

(b) Legend including euclidean error norm [mm]. (Theoretical minimum in gray)

Figure 4.16: Closed-loop performance straight cone.

4.4.4 Closed-loop Robustness

In the previous results, the MPC was tested on the same perfect Finite Element model as the control models were determined with. In practice, parameters may have a certain variance or may not be exactly known and not all physical phenomena might be modelled. Therefore, the MPC is tested on Finite Element models with varying parameters in this section.

Randomized parameters

To model disturbances in the process, random parameters have been given to the Finite Element simulation on which the MPC was tested. The values have been randomly generated between reasonable bounds and can be seen in Table 4.1.

Parameter	**Nominal value**	**Range**	**Randomized set 1**	**Randomized set 2**
Thickness [mm]	1	0.75-1.25	1.21	0.99
Friction μ	0.05	0-0.1	0.058	0.086
Stiffness k [N/m]	∞	10^8-10^9	$7.92{\cdot}10^8$	$2.09{\cdot}10^8$
Hardening coefficient C	390	350-430	396.4	417.6
Hardening exponent n	0.19	0.18-0.20	0.18	0.18

Table 4.1: Randomized parameter values

Figure 4.17 shows the result of a closed-loop MPC run on a model with the parameters from set 1. The results for set 2 can be found in appendix E.1. The light grey dashed line indicates the error when following the nominal toolpath in a model with nominal parameters. The black dashed line indicates the error when following the nominal toolpath in a model with the random parameter set. The error values are very close to each other, but significantly lower than the normal closed-loop run, which is surprising. This difference is mainly due to the reduction of error at the outside of the product.

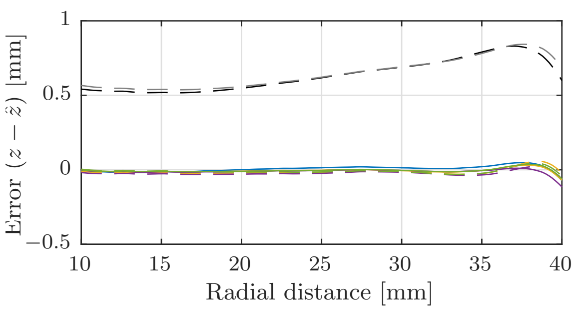

(a) Error from target

	Assumed control direction	
Impulse response definition	Positive Δu (——)	Negative Δu (- - -)
- - Nominal parameters	8.03	
- - Random parameters	7.89	
— 1 - Full nom. step	0.24 (0.12)	
— 3 - Resp. at N_t	0.17 (0.12)	0.28 (0.10)
— 4 - History	0.22 (0.12)	0.32 (0.10)
— 5 - Weibull fit	0.17 (0.12)	0.22 (0.12)

(b) Legend including euclidean error norm [mm]. (Theoretical minimum in gray)

Figure 4.17: Robustness to random parameter set 1 in closed-loop.

Setup stiffness

A well-known problem in the use of CNC setups is the compliance of the structure on which the tool is attached. Pan et al. [29] stated that a linear CNC setup generally has a stiffness in the order of 10^8 N/m where an industrial robot has a stiffness of around 10^6 N/m. The large influence of compliance in the usage of industrial robots has been recognized and researched by several researchers [30,31], which show results in the same order of magnitude. In the FE-model, the stiffness of the setup is modelled as a spring attached to the tool that can only deform in one direction. The reference point for the tool path is now the loose end of the spring.

Figure 4.18 shows the control actions applied in a closed-loop run with a stiffness of 10^6 N/m. It can be seen that the required corrections are around 2 mm larger than in the closed-loop run with nominal parameters, which is what can be expected with process forces in the order of kilonewtons.

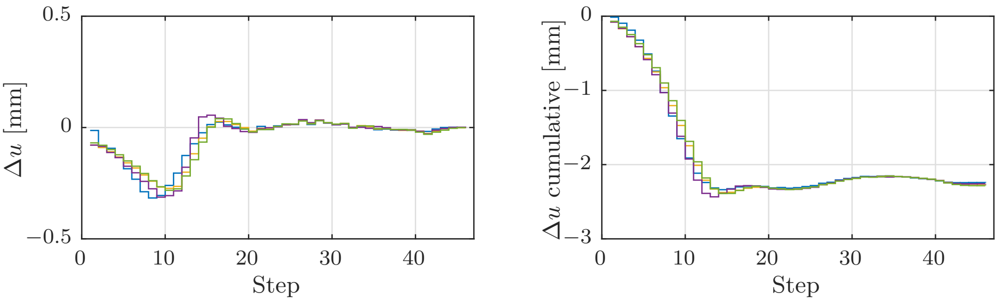

a) Models defined by applying a positive Δu

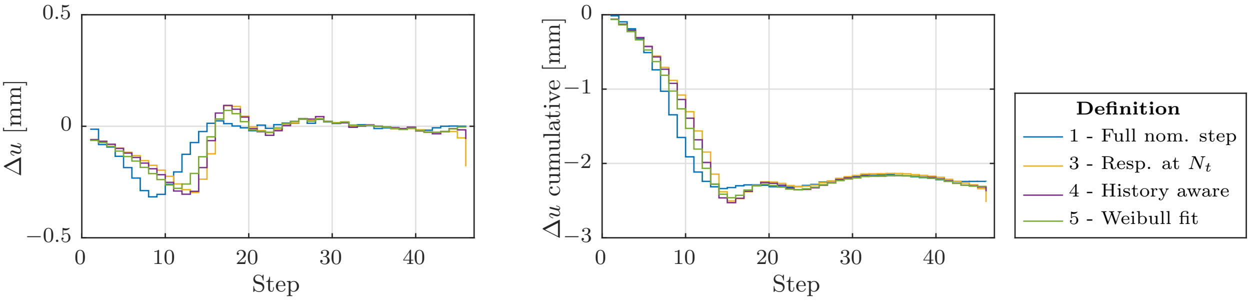

b) Models defined by applying a negative Δu

Figure 4.18: Closed-loop strategy for a setup with low stiffness.

The black dashed line in fig. 4.19 indicates that the error when following the nominal toolpath on a compliant setup is indeed roughly 2 mm larger than when an infinitely stiff setup is modelled. Despite the low stiffness, the MPC still succeeds in reducing the error. However, some oscillation of the error can be observed when using control models determined with negative Δu. What stands out is the error norm of *Def. 4 - History aware* . This error is lower than in the analysis with nominal parameters and very close to the theoretical minimum.

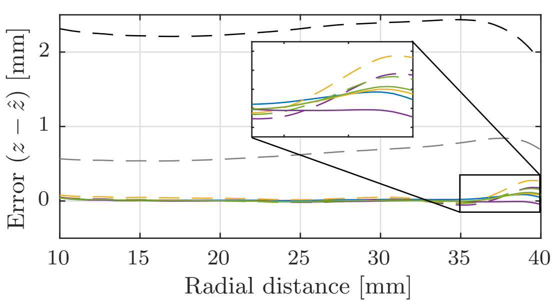

(a) Error from target

	Assumed control direction	
Impulse response definition	Positive Δu (—)	Negative Δu (- - -)
- - Nominal parameters	8.03	
- - Random parameters	28.23	
— 1 - Full nom. step	0.35 (0.12)	
— 3 - Resp. at N_t	0.35 (0.12)	0.98 (0.10)
— 4 - History	0.14 (0.12)	0.59 (0.10)
— 5 - Weibull fit	0.39 (0.12)	0.54 (0.12)

(b) Legend including euclidean error norm [mm]. (Theoretical minimum in gray)

Figure 4.19: Robustness to a low setup stiffness in closed-loop.

4.4.5 Application to similar target geometries

The extension of the linearisation is this thesis makes that the computational effort to construct the control models is increased. It might therefore be desirable if it is not required to construct a new control model for every new product. In the following section, a cone with two different wall angles will be formed with a toolpath close to that of the single wall angle cone, in order to investigate whether the process model of a closely related product is sufficiently accurate for use in Model Predictive Control.

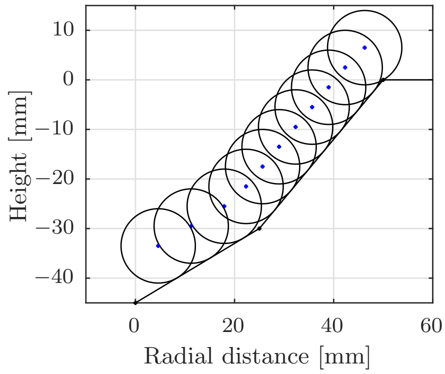

Figure 4.20: One-step cone target geometry. The circles represent a part of the tool locations.

New target

A simple approach would be to feed the MPC the new target of the one-step cone, as shown in fig. 4.20, without changing the nominal toolpath, impulse response models and nominal state evolution. To reach this new target, the MPC has to make large corrections. Therefore, the performance of this analysis indicates how valid the assumption of the linearity of the control actions is and to what extent the developed linearisation can successfully be used.

Figure 4.21 shows the resulting error of an MPC run on the one-step cone target. Most noticeable is the bad performance of *Def. 1 - Full nom. step* and models determined with negative Δu. Promising is the performance of Definitions 3, 4 and 5 determined with a positive Δu . The largest error is located around the transition in wall angle, where the process can not create the sharp wall transition due to the tool radius. In the other regions, the error is close to zero.

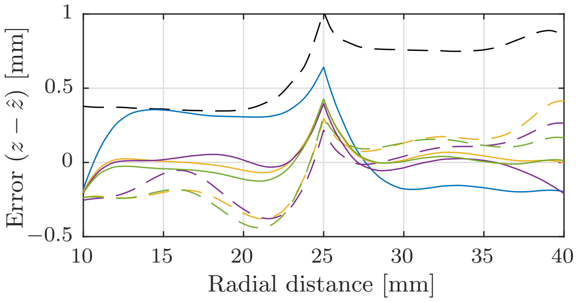

(a) Error from target

Impulse response definition	Assumed control direction: Positive Δu (——)	Negative Δu (- - -)
- - No control	7.93	
— 1 - Full nom. step	3.40 (0.85)	
— 3 - Resp. at N_t	1.14 (0.84)	2.86 (0.82)
— 4 - History	1.14 (0.84)	2.27 (0.82)
— 5 - Weibull fit	1.23 (0.86)	2.73 (0.87)

(b) Legend including euclidean error norm [mm]. (Theoretical minimum in gray)

Figure 4.21: Closed-loop performance new target (one-step cone).

To reach the new target geometry, large positive control actions have to be applied (see fig. E.2 in appendix E.1). This might contribute to the large error norms for models determined with negative Δu.

New target and approximated nominal state evolution

All toolpaths in this thesis are calculated using the contour following method. With the contour following path of the one-step cone geometry, the deviations Δu from the straight cone toolpath necessary to follow the one-step cone toolpath can be calculated. With the developed linearisation, the state at each time step when following this toolpath can be predicted and used as nominal state evolution $\bar{z}$ in the MPC. This has as a result that the MPC only has to make small corrections on this new toolpath. The nominal state evolution of the one-step cone ($\bar{\boldsymbol{z}}'$), indicated by the prime, can be predicted using:

$$\bar{\boldsymbol{z}}'_{k+1} = \bar{\boldsymbol{z}}_{k+1} + \sum_{j=1}^{k} \boldsymbol{g}_j \Delta u'_j \qquad \text{,where:} \quad \Delta \boldsymbol{u}' = \boldsymbol{u}' - \boldsymbol{u} \tag{4.4}$$

With $\boldsymbol{u}'$ being the vector containing vertical step heights of the new geometry and $\boldsymbol{u}$ being the vector containing step heights of the old geometry. *Def. 3 - Resp. at N_t* determined with positive Δu is used to predict the nominal state evolution of the one-step cone.

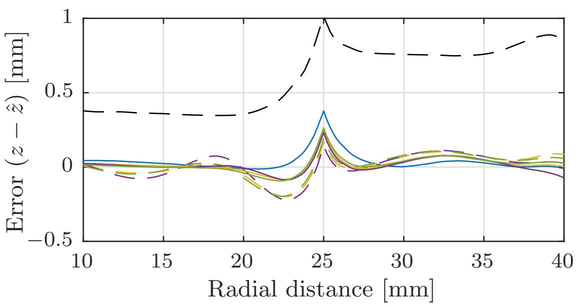

(a) Error from target

Impulse response definition	Assumed control direction: Positive Δu (—)	Assumed control direction: Negative Δu (- - -)
- - No control	7.93	
— 1 - Full nom. step	0.92 (0.60)	
— 3 - Resp. at N_t	0.63 (0.61)	0.96 (0.62)
— 4 - History	0.61 (0.61)	1.02 (0.62)
— 5 - Weibull fit	0.70 (0.57)	0.99 (0.57)

(b) Legend including euclidean error norm [mm]. (Theoretical minimum in gray)

Figure 4.22: Closed-loop performance new target (one-step cone) using an approximated state evolution.

Figure 4.22 shows the results of a closed-loop MPC run using the new toolpath, new target and approximated state evolution. A significant improvement compared to only using a new target can be seen. The models determined with positive Δu perform very close to the theoretical minimum. The models determined with negative Δu cause an oscillating error after the wall-angle transition, which results in a larger error norm.

New target and exact nominal state evolution

As a reference, the MPC with the new target and new path has also been tested using the exact state evolution corresponding to the new path. A Finite Element analysis of the new toolpath has been performed and the resulting states have been used as the nominal state in the MPC. The same impulse response model as in the other analyses is used.

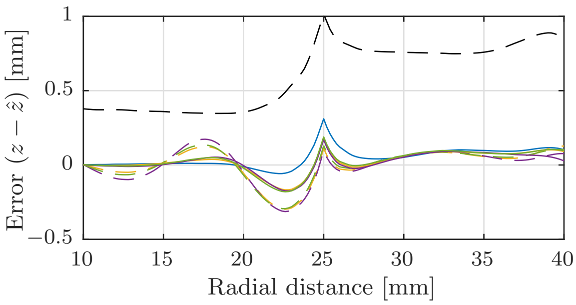

(a) Error from target

Impulse response definition	Assumed control direction: Positive Δu (——)	Assumed control direction: Negative Δu (- - -)
- - No control	7.93	
— 1 - Full nom. step	0.98 (0.53)	
— 3 - Resp. at N_t	0.89 (0.52)	1.30 (0.51)
— 4 - History	0.85 (0.52)	1.42 (0.51)
— 5 - Weibull fit	0.94 (0.51)	1.32 (0.51)

(b) Legend including euclidean error norm [mm]. (Theoretical minimum in gray)

Figure 4.23: Closed-loop performance new target (one-step cone) using the exact state evolution.

Figure 4.23 shows the results of this analysis. The results are comparable with the previous analysis using the approximated state evolution. Surprising is the slightly higher error for all models than when using the approximated state evolution. Again, some oscillation of the error can be observed for impulse response models determined with negative Δu.

4.4.6 Analysis of oscillating error

The use of control models determined with negative Δu (deeper toolpath) generally resulted in a less accurate final geometry or an oscillating error in the case of large control actions. The origin of this problem can be found in the radial shift of the impulse response for different values of Δu. The analysis on linearity in section 4.3.1 showed that the impulse response moves radially outwards with lower values of Δu.

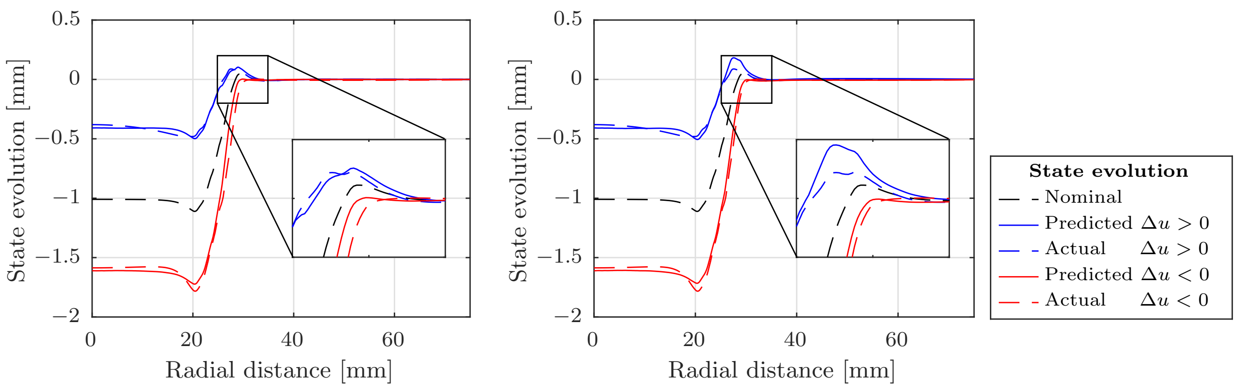

(a) $\boldsymbol{G}$ determined using Δu = 0.6 mm **(b)** $\boldsymbol{G}$ determined using Δu = -0.6 mm

Figure 4.24: Difference in predicted state evolution and actual state evolution due to using a control model determined with a Δu of another direction than the Δu applied. The process model has been used to predict the instant effect from step k (25) to step $k+1$ (26) as a result of applying $\Delta u_{25} = \pm 0.6$ mm. The control model $\boldsymbol{G}$ is determined using *Def. 3 - Resp. at N_t* .

When the model determined with negative Δu is used to predict the state evolution for a positive Δu, the blue solid line in fig. 4.24b is the result. The dashed line represents the actual result of applying such a control action. In the magnification, the figure shows that the model predicts a large positive response near the edge of the tool, where in reality, the positive response is lower. This means that the MPC algorithm thinks that it has the ability to form the product back upwards at this location by applying a positive control action. However, this does not happen in practice. As this model inaccuracy is present exactly at the transition between the region that can still be corrected by future control actions, and the region that will be out of reach of the MPC after this step, it is highly probable that the MPC will try to make use of this incorrect feature in the process model. This can result in oscillation of the error and gets more severe at large magnitudes of control actions.

4.5 Conclusion

In this chapter, the applicability of the developed process model on simple axisymmetric products has been investigated. Analysing the different definitions of the impulse response model gave new insights that led to the development of *Def. 4 - History aware* . Testing the MPC made clear that the different definitions of the impulse response model and the direction of the correction with which they are determined have a large effect on the accuracy of the control system. However, the differences in error are small and the MPC reduces the error significantly compared to having no control in all cases, while being robust to parameter variation and being able to steer the process to slightly different target geometries than the process model is linearised on.

5 Complex products

In the previous chapter, the developed theory in chapter 3 was tested on simple and insightful axisymmetric geometries. In the following chapter, the same theory is tested on a more complex target geometry. It is investigates how well the impulse response models work for complex target geometries and for toolpath corrections in another direction than perpendicular to the z-level contour.

5.1 Methodology

The products in this chapter are created by a series of rectangular z-level contours. The process can not easily be reduced to a 2D problem by axisymmetry, which makes it desirable to correct the toolpath at multiple control points along 1 z-level contour.

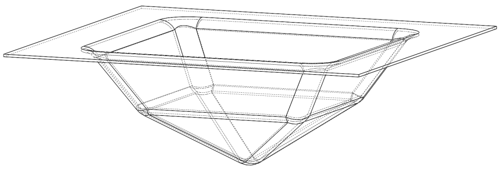

Figure 5.1: Two-angle pyramid geometry

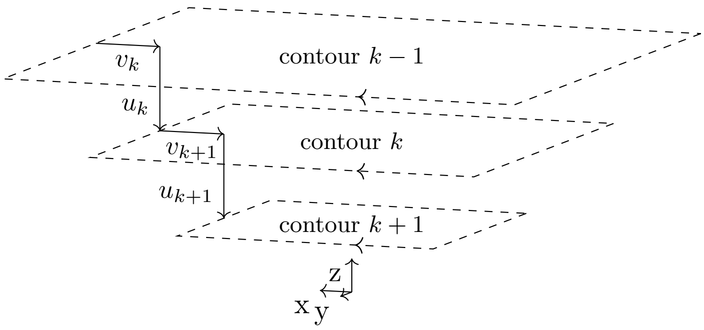

Figure 5.2: Path definition

Each time step k in the process contains 1 z-level rectangular contour, as schematically displayed in fig. 5.2. In products containing rectangular or more free-form z-level contours, it might be beneficial to switch to radial control of multiple control points on 1 contour. In radial control, the toolpath is only corrected in the plane of the z-level contour itself to keep the contour two-dimensional. This approach can be combined with vertical control of the whole z-level contour. To distinguish radial and vertical control, the radial step between contours will be named v_k and the vertical step will be named u_k. v_k is defined as:

$$v_k = r_k - r_{k-1} \tag{5.1}$$

Where r is the radial distance to a control point on the contour. The inaccuracy in products formed by rectangular contours is the largest at the flat faces. The corners are generally well-formed due to the stiffness obtained in a corner. Therefore, the control action Δv is only applied in the middle of the faces as schematically shown in fig. 5.3. The contour is linearly interpolated between the nominal path in the corners and the corrected path in the middle of the faces. Note that the schematic shows a single correction. Since the step size is corrected instead of the actual location of the contour, it can move away far from its initial position when multiple corrections in the same direction are done.

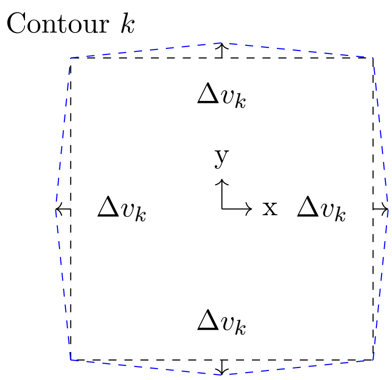

Figure 5.3: Definition of radial control actions for rectangular contours

Whenever vertical control (Δu) is applied in this chapter, the whole contour k is vertically corrected. This causes an error in the corners, but can give valuable insights in the performance of the MPC on the middle of the flat faces, which is the error which will be focussed on.

5.2 Nominal analysis

A shape that is known to give problems in accuracy is the two-angle pyramid which is shown in fig. 5.1. The process will be linearised around the contour-following toolpath corresponding to the two-angle pyramid. The sheet has a size of 150x150 mm and is clamped around the edges. The nominal step height between the contours is $\bar{u}$ = -1 mm and the tool radius is 5 mm. As the error will most likely be the highest at the flat faces of the pyramid, the state of the product is only sampled in the middle of theses faces, at lines $x = 0$ and $y = 0$. This sampling is visualized in fig. 5.5. When sampled at these locations, the target geometry in fig. 5.1 reduces to fig. 5.4.

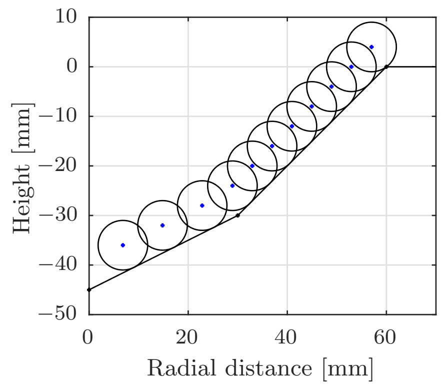

Figure 5.4: Two-angle pyramid target geometry. The circles represent a part of the tool locations.

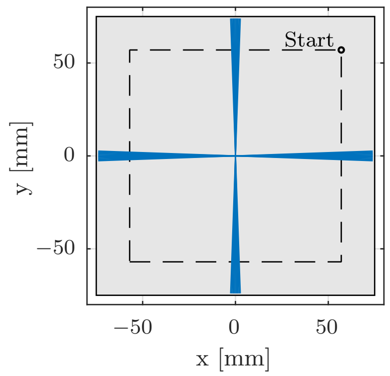

Figure 5.5: Sampling of products formed by rectangular contours. The deflection (state $\boldsymbol{z}$) is averaged over the blue lines.

Figure 5.6 shows the errormap of the final geometry when following the nominal path obtained by the contour-following method. As can be seen, the area around the wall-angle transition indeed contains a large error on the flat faces (red). Another large error is global bending near the clamping due to the lack of support (blue). As expected, the corners are well formed and only contain small errors.

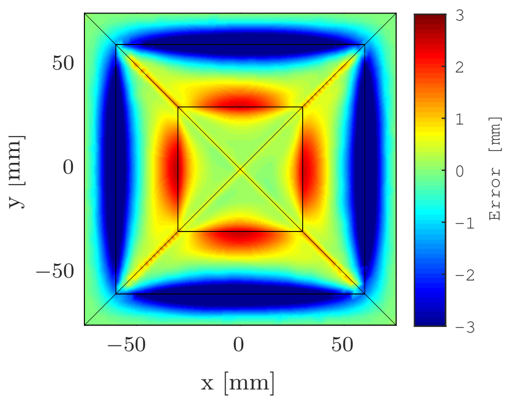

Figure 5.6: Error map of the two-angle pyramid when using the nominal toolpath.

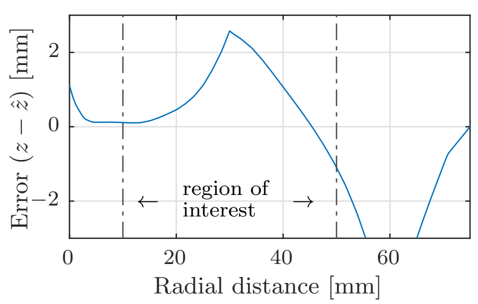

Figure 5.7: Error when the product is sampled according to fig. 5.5.

If the error map is sampled as shown in fig. 5.5, the error in fig. 5.7 is the result. The error far below zero represents global bending of the product and can hardly be reduced by toolpath optimization. The error at the inside of the product is the result of the tool not being able to form a perfectly sharp pyramid due to its radius. Therefore, these regions are excluded from the analysis and the product state is only evaluated in the region of interest as depicted ($10 \leq r \leq 50$ mm).

Figure 5.8 shows the resulting height after every step. The red line marks the final geometry. The magnification shows that the error in the region where the wall angle changes is initially smaller, but increases during subsequent forming passes. This can also be seen in the impulse responses in fig. 5.9, which become negative on radii greater than the tool location.

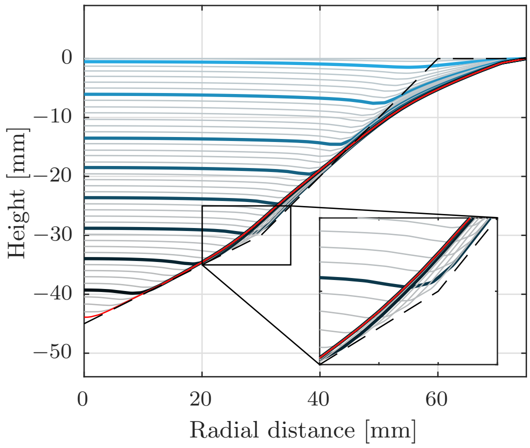

Figure 5.8: Height z_{k+1} after each step k (red = final geometry).

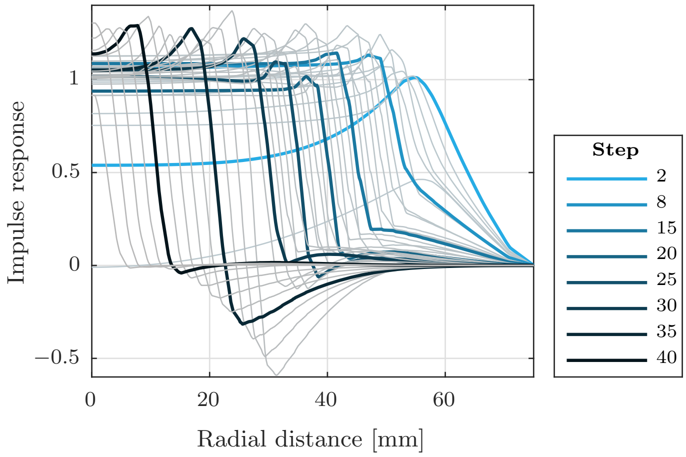

Figure 5.9: Impulse response g_k according to *Def. 1 - Full nom. step*

The phenomenon was first observed by Behera et al. [19] and named the "tent-effect". The effect is problematic for control, since this change in shape only occurs a few steps after the tool has passed, which makes it impossible to correct it afterwards. This underlines the importance of a model that is able to predict accurate deformations, also in regions that are not accessible by the tool anymore.

5.3 Impulse response analysis

The impulse response model for products produced by rectangular contours is constructed in the same fashion as for the products produced by circular contours in chapter 4. The effect of a control action on the product state can be investigated regardless of the direction of control or number of control points per z-level contour. In this chapter, only *Def. 3 - Resp. at* N_t and *Def. 4 - History aware* are used, since *Def. 1 - Full nom. step* and *Def. 2 - Resp. at* $k+1$ do not capture the effect of a radial control action on the final geometry and a Weibull curve can not be fitted to the models.

5.3.1 Linearity

As explained in section 2.3.1, it is important that the impulse response is linear with the magnitude of the control action. The linearity is checked at a step on each wall-angle. Step 20 corresponds to the first steep wall angle and step 35 corresponds to the second, less steep, wall angle.

Radial control

Figure 5.10 shows the linearity of impulse response *Def. 3 - Resp. at* N_t for radial control. Both shape and magnitude are not perfectly linear. The most severe non-linearity is observed in the tool region, where outside the tool region the non-linearity seems to be a radial shift due to the radial shift of the tool. This effect should be accounted for by a radial shift of the linearisation, as will be explained in section 5.4.2.

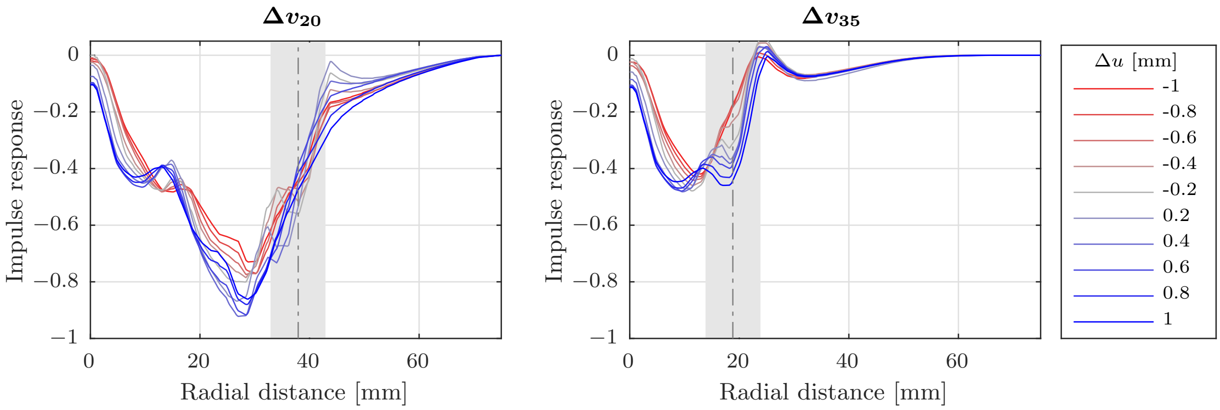

Figure 5.10: Linearity of impulse response *Def. 3 - Resp. at* N_t for radial control.

Vertical control

Figure 5.11 shows the linearity of impulse response *Def. 3 - Resp. at* N_t for vertical control. In the responses at step 35, an unusual large shift in impulse response for negative Δu is observed, which can cause problems when an impulse response model determined with negative Δu is used. Similar to the linearity analysis for axisymmetric products, the assumption of linearity seems to hold well for vertical control of the pyramid product in the other regions.

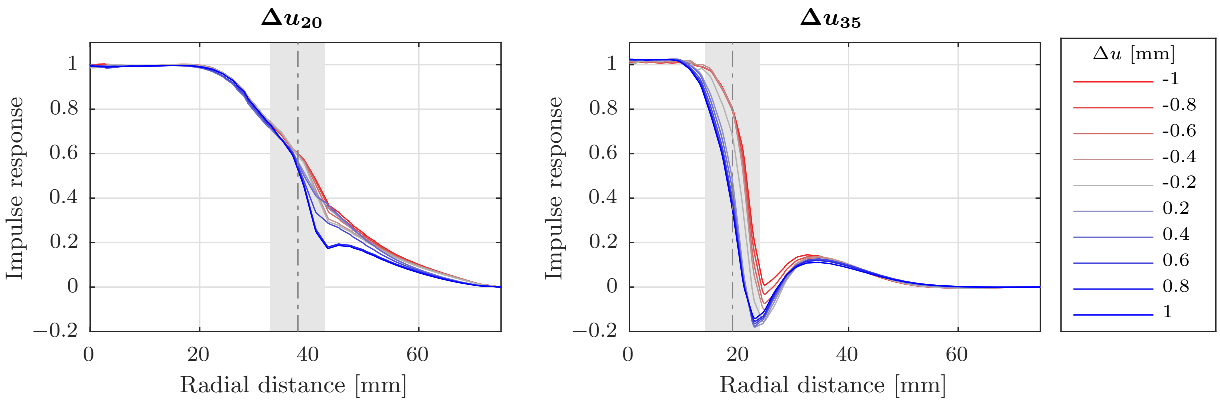

Figure 5.11: Linearity of impulse response *Def. 3 - Resp. at* N_t for vertical control.

5.3.2 Time-consistency

For vertical control, the state over time of a corrected analysis can be compared with the nominal analysis, similar to section 4.3.2. These results can be found in appendix D. The information from this analysis can be rewritten to *Def. 4 - History aware* to be used in the MPC, as described in appendix B.1.

For radial control, this is less straightforward. The radial correction on the tool causes the impulse response to shift, which means that this shift should be accounted for in the comparison with the nominal process. Furthermore, applying the theory of shifting the response on *Def. 4 - History aware* will create a complex non-linear formulation in the MPC, which is undesirable. Therefore, *Def. 4 - History aware* is not usable for radial control.

5.3.3 Control models

The following section presents the control models that will be used when testing the MPC in section 5.4. The models of for both radial and vertical control will be determined by applying a correction of ±0.5 mm, as the MPC will also be bounded to corrections of ±0.5 mm.

Radial control

In contrast with vertical control on the straight cone, radial control on the walls of the pyramid is very different for positive and negative Δv. This has three reasons. The direction of the control action is not in the direction of forming (perpendicular to the sheet), the tent-effect affects the final geometry and because only the sides of the pyramids are controlled, the corners could interfere and prevent the flat faces from deviating from their nominal state.

A few important details can be seen in the figures below, where the impulse responses determined with positive and negative Δu are shown. First of all, for both control directions, the shape of the impulse responses for the first steps, on the steep wall-angle, has roughly the same shape. This shape is very wide and thus has an effect on a large part of the product, where in vertical control the response of a control action is only seen in a specific region of the product. This makes that for vertical control, a specific effect is bounded to a single step, where in radial control, multiple steps have roughly the same effect. This can affect the "choices" made by the MPC. Another important feature is the impulse response above zero for a positive control action. This means that the tent-effect is more severe at that location than when following the nominal path.

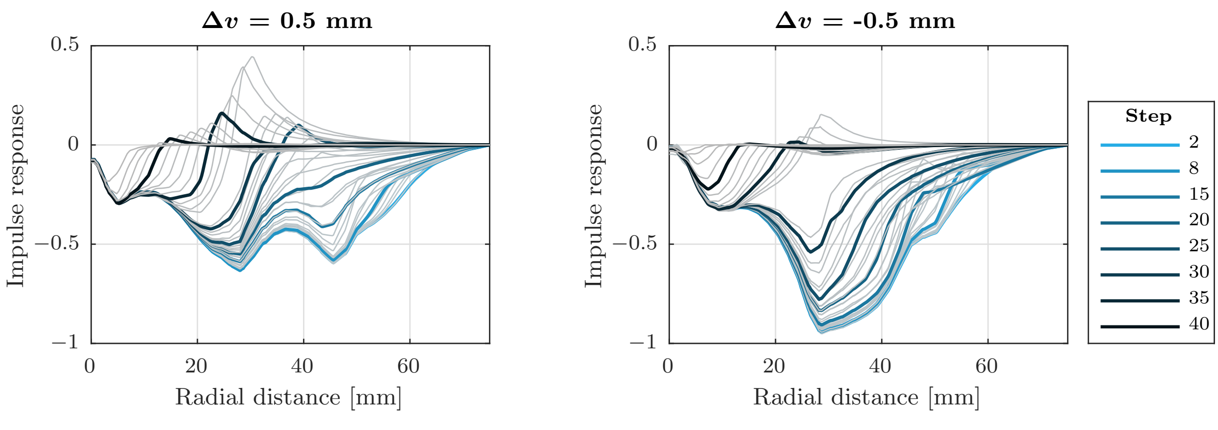

Figure 5.12: Impulse response *Def. 3 - Resp. at N_t* for radial control. Determined with $\Delta v = \pm$ 0.5 mm

Vertical control

The impulse responses in vertical control of the pyramid are much more similar to the impulse responses encountered when forming the cone. The large difference is again in the first steps on the first, steep wall-angle. The response is very wide here and has roughly the same shape and location for a lot of steps. This again indicates that the effect is very widespread and that a desired effect is not bounded to one specific control action.

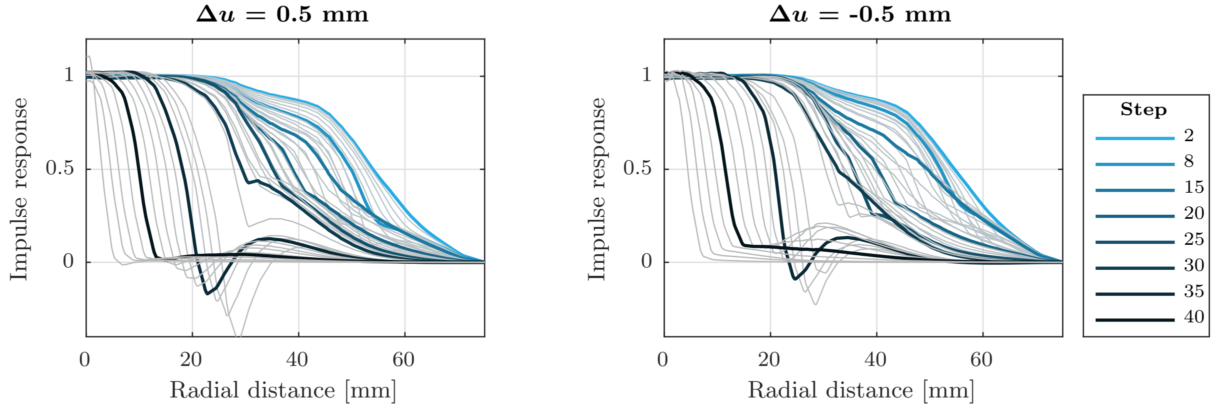

Figure 5.13: Impulse response *Def. 3 - Resp. at N_t* for vertical control. Determined with $\Delta u = \pm$ 0.5 mm

5.3.4 Large vertical deviations from the nominal path

Similar to the approach in section 4.3.2, the effect of control actions in the past can be gathered and added to the linear system as explained in section 3.2. The term in *Def. 4 - History aware* containing the influence of control actions in the past ($\boldsymbol{Q}_{his,k}\Delta\boldsymbol{u}_{his,k}$) can be seen as a correction on the nominal state evolution. The nominal state evolution $\bar{\boldsymbol{z}}_{N_t} - \bar{\boldsymbol{z}}_k$ is what can be expected in the remaining of the process when no additional corrections on the toolpath would be done.

To check the validity of this linearisation, a process has been performed with corrections on the step height during a number of time steps, after which the process continues without corrections, following the nominal path. The state evolution of the corrected path can be compared with the state evolution following the nominal path. The difference should be captured by the term that accounts for control actions in the past in *Def. 4 - History aware* .

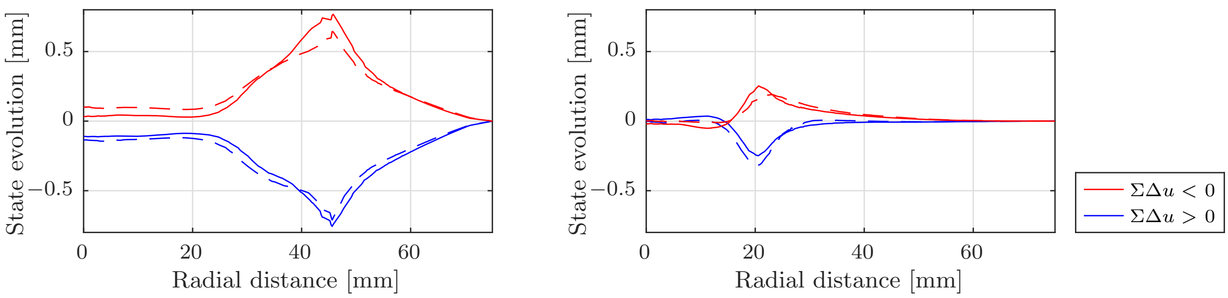

(a) Corrected from step 1 to step 15 **(b)** Corrected from step 21 to step 35

Figure 5.14: Effect of control actions in the past on the nominal state evolution. The solid lines represent the actual difference from the nominal state evolution after deviating from the nominal toolpath. The dashed lines represent the correction taking into account the control actions in the history ($\boldsymbol{Q}_{his,k}\Delta\boldsymbol{u}_{his,k}$).

Figure 5.14 shows the results of such an analysis. In the nominal analysis, no control actions were applied. In the left figure, positive and negative control actions $\Delta u = \pm 0.15$ were performed from step 1 to step 15 ($\Delta u_i = \pm 0.15\text{mm} \quad \forall i \in \{1, 2, \ldots, 15\}$) in two separate analyses. In the right figure, positive and negative control actions $\Delta u = \pm 0.15$ mm were performed from step 21 to step 35 ($\Delta u_i = \pm 0.15\text{mm} \quad \forall i \in \{21, 22, \ldots, 35\}$) to investigate the same effect on the other wall angle.

The solid lines in Figure 5.14 show the difference between the actual state evolution after deviating from the nominal path ($\boldsymbol{z}_{N_t} - \boldsymbol{z}_{16}$ and $\boldsymbol{z}_{N_t} - \boldsymbol{z}_{36}$) and the nominal state evolution ($\bar{\boldsymbol{z}}_{N_t} - \bar{\boldsymbol{z}}_{16}$ and $\bar{\boldsymbol{z}}_{N_t} - \bar{\boldsymbol{z}}_{36}$). The dashed lines represent the deviation from the nominal state evolution as predicted by *Def. 4 - History aware* ($\boldsymbol{Q}_{his,k} \Delta \boldsymbol{u}_{his,k}$). The dashed and solid lines are similar and close to each other, which indicates that the correction taking into account control actions in the past is a valid approach.

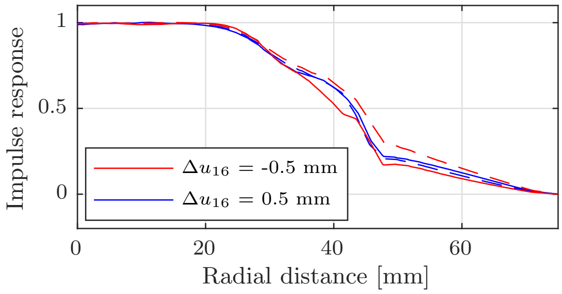

(a) Corrected from step 1 to step 15

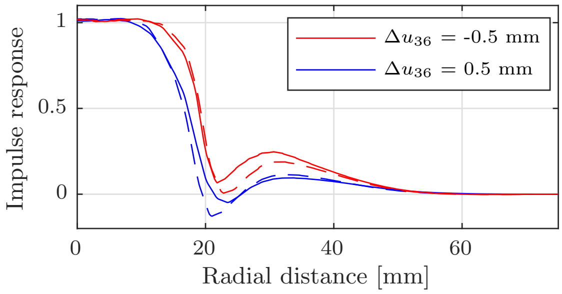

(b) Corrected from step 21 to step 35

Figure 5.15: Effect of control actions in the past on the impulse response (*Def. 3 - Resp. at N_t*). On the left corrections from step 1 to step 15, on the right corrections from step 21 to step 35.

When large deviations from the toolpath are made, the validity of the impulse response models is also questionable. Therefore, an additional correction of 0.5 mm on the deviated toolpath is done in a separate analysis to determine the effect of a correction on the final geometry when deviated from the path ($\Delta u_{16} = \pm$ 0.5 mm and $\Delta u_{36} = \pm$ 0.5 mm). In other words, this is the effect of already performed control actions, that only becomes visible during later forming steps, instead of directly after these control actions were applied. The final geometry of these analyses is compared to the final geometry of the analysis in which deviations from the toolpath were made from step 1 to 15 and step 21 to 25 using *Def. 3 - Resp. at N_t* . The solid line in Figure 5.15 gives the impulse response when deviated from the toolpath and the dashed line represents the impulse response when determined at the nominal toolpath. Small differences can be observed, especially for the deviations later in the process in fig. 5.15b, but the impulse response shape remains similar. It is expected that the MPC can deal with this model error.

5.3.5 Radial impulse response shift

Figure 2.6 shows that the impulse response moves radially inwards over time, which can be explained by the radial movement of the tool. When a vertical control action Δu is applied, the radial location of the tool does not change and it can be assumed that the validity of the impulse response model still holds. When the toolpath is corrected with a radial control action Δv, the tool location changes radially for the current and all coming steps. Since the deformation is related to the radial position of the tool, a solution could be to shift the impulse response model and nominal state evolution ($\bar{\boldsymbol{z}}_{N_t} - \bar{\boldsymbol{z}}_k$) by an offset of $\Sigma \boldsymbol{\Delta v_{his}}$. The impulse response has been related to the tool location by other researchers [23, 24] In the following analyses, it is investigated whether the nominal state evolution can also be related to the tool location.

Figure 5.16 shows the results of two analyses in which the state evolution after applying radial control actions is compared with the nominal state evolution. In the left figure, $\Delta v_i = \pm 0.15\text{mm} \quad \forall i \in \{1, 2, \ldots, 15\}$ and the state evolution is compared from step 16 to the end $(\boldsymbol{z}_{N_t} - \boldsymbol{z}_{16})$. In the right figure, $\Delta v_i = \pm 0.15\text{mm} \quad \forall i \in \{21, 22, \ldots, 35\}$ and the state evolution is compared from step 36 to the end $(\boldsymbol{z}_{N_t} - \boldsymbol{z}_{36})$.

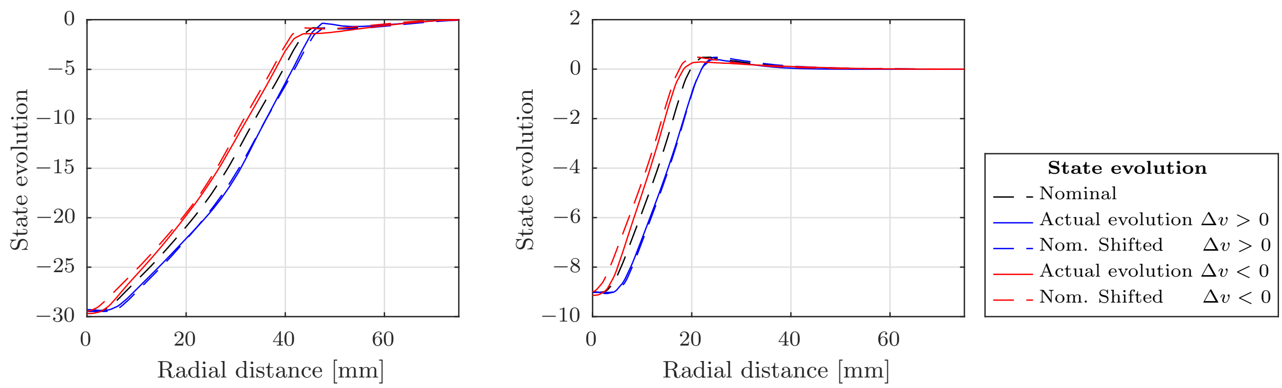

(a) State evolution after step 16

(b) State evolution after step 36

Figure 5.16: Analysis of the state evolution after a series of control steps. The solid line indicates the actual shift of the state evolution after applying radial control. The dashed lines represent the expected shift of the nominal state evolution.

The theory on shifting the terms in the linearisation radially assumes that the nominal state evolution should now be shifted by 2.25 mm, which is the sum of the control actions applied. In fig. 5.16, the dashed line represents the shifted nominal state evolution and the solid line represents the actual state evolution after applying control. It can be seen that for both cases the assumption holds well for positive control action, but less well for a negative control action at the inside of the product. This does not have to be a problem since most products have a positive error, meaning that they are underformed and the cumulative control actions will probably be positive in the case of radial control, resulting in a deeper toolpath.

5.4 MPC Performance

5.4.1 Methodology

The MPC in this chapter only focusses on the error in the middle of the faces of the pyramid, as presented in fig. 5.5. Similar to the MPC in the chapter 4 on axisymmetric products, only the spatial discretization points in the region of interest will be used. The region of interest is ($10 \leq r \leq 50$ mm) in this case. The error will be plotted and measured with the euclidean error norm as shown in eq. (4.3)

Unless mentioned otherwise, the MPC is run with weight factor $\alpha = 16$ for radial control and $\alpha = 8$ for vertical control. The bounds for both vertical and radial control are $-0.5 \leq \Delta u \leq 0.5$ mm and $-0.5 \leq \Delta v \leq 0.5$ mm. In radial control an additional constraint is applied to ensure that the radial coordinate of the tool does not become negative at the end:

$$\sum_{i=1}^{N_t-1} \Delta v_i \geq 0 \tag{5.2}$$

The applied control actions for all models and directions of control will not be given in this chapter, but can be found in appendix E.2

5.4.2 Radial shift of the impulse response

As explained in section 5.1, it might be beneficial to switch to radial control when forming more complex products. The analysis in section 5.3.5 showed that the nominal state evolution and impulse response model shift radially when radial control actions are applied. This makes the impulse response model and nominal state evolution invalid. A solution is to shift these terms in the linearisation radially. Two methods are proposed:

Shift 1 - Total response matrix In method 1, all impulse responses which are used in the MPC at the current time step are radially translated by the sum of all radial control actions in the past. This method does not account for all control actions to be done in the future. This does not necessarily have to be a problem since only the first control action in the optimized sequence is actually applied in MPC.

Shift 2 - Every response A more accurate prediction can be made by shifting every impulse response according to the corresponding Δv. However, this makes the linearisation dependent on Δv, which means that the optimization problem can not be reduced to the standard QP formulation. A general (non-linear) optimization algorithm should be used which calculates the cost function in the MPC as a result of the proposed strategy $\boldsymbol{\Delta v}$.

5.4.3 Radial control

In the following section, the results of radial control of the toolpath by the MPC are presented. The toolpath is corrected as schematically shown in fig. 5.3.

Open-loop

When the MPC is ran in open-loop, the complete strategy $\boldsymbol{\Delta v}$ as determined on step $k = 1$ is applied to the nominal path. Since state feedback is not used here, the analysis gives an indication of the model error in the linearisation. Figure 5.17a shows the output of the MPC when ran at step $k = 1$, which leads to the path correction as shown in fig. 5.17b. Since in open-loop, no history of control actions $\boldsymbol{\Delta v}_{his}$ is available yet, the impulse response and nominal state evolution are not shifted.

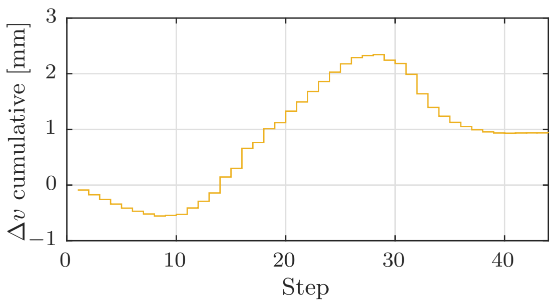

(a) Cumulative Δv strategy

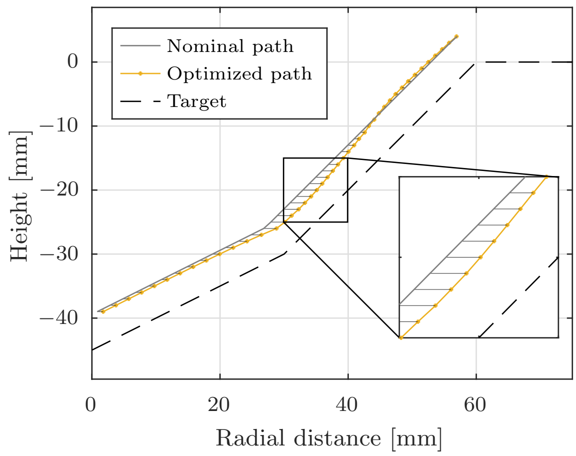

(b) Corrected path

Figure 5.17: Open-loop MPC output using *Def. 3 - Resp. at N_t* determined with positive Δv.

Figure 5.18 shows the resulting error of the strategy presented in fig. 5.17. Against expectations, the error is very low. In open-loop, the radial shift of the tool is not accounted for, which should result in large model error. The low geometric error in Figure 5.18 indicates that this is not a large problem in open-loop. The error norm values in the table even indicate that the error is lower than theoretical minimum that the MPC predicts. This feeds the thought that the model error turned out to be favourable for the control system by chance.

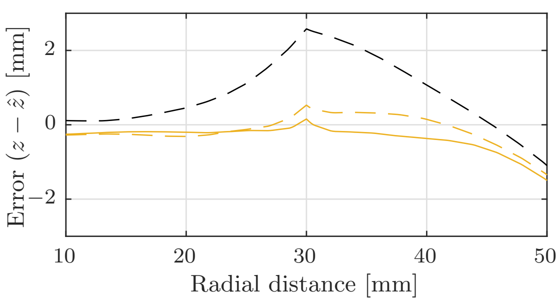

(a) Error from target

	Assumed control direction	
Impulse response definition	Positive Δv (——)	Negative Δv (- - -)
- - No control	17.74	
— 3 - Resp. at N_t	6.43 (7.90)	5.75 (6.10)

(b) Legend including euclidean error norm [mm]. (Theoretical minimum in gray)

Figure 5.18: Open-loop performance when using radial control on the two-angle pyramid.

It can also be seen that a control model determined with negative Δv yields more accurate results than a control model determined with positive Δv. This is in agreement with most results since a negative Δv corresponds to a less deep path, where a negative Δu corresponds to a deeper path.

Closed-loop

In the numerical environment of this thesis, the control system is determined using the same finite element model as it is tested on. An open-loop approach might seem promising, but will most likely fail in a real system due to model error and disturbances. Therefore, a good closed-loop performance is desirable. When radial control is used closed-loop, the terms in the linearisation should be radially shifted because of the radial deviation from the nominal path by the tool, as explained in section 5.4.2.

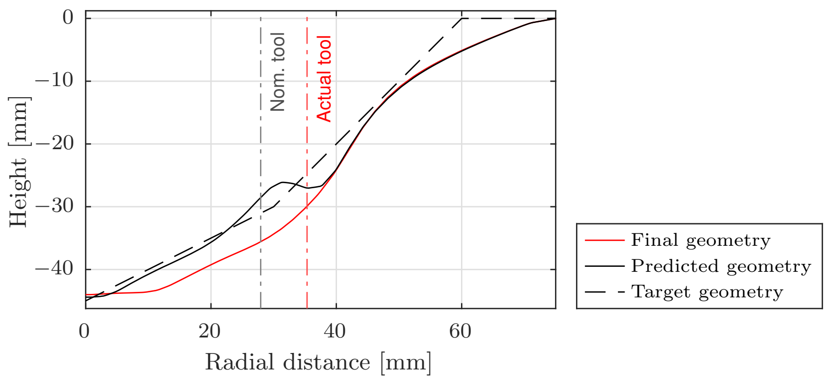

Figure 5.19: Difference between the predicted optimal geometry at step 30 and actual result due to tool shift. The response model used is determined using *Def. 3 - Resp. at* N_t .

When this is not done, the effect of a process step is predicted at the wrong radial location. Figure 5.19 shows the difference between the optimal final geometry as predicted by the process model at step 30 and the actual final geometry when following the optimal strategy. The linearisation predicts at step 30 that the tool will have an effect from 0 to 30 mm, while the tool actually deviated from the toolpath and now has an effect from 0 to 35 mm. As a result, the state will deviate from the target state and require larger control actions after each step. The MPC will run to its bounds and the resulting final geometry will contain a large error.

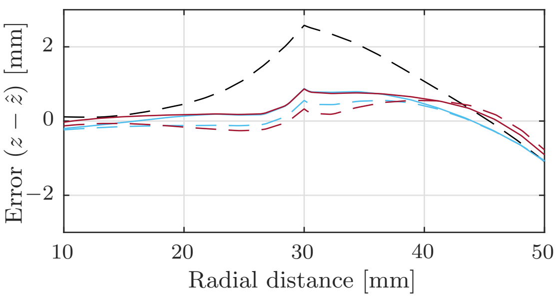

(a) Error from target

	Assumed control direction	
Impulse response definition	Positive Δv (—)	Negative Δv (- - -)
- - No control	17.74	
— Shift total response	6.65	5.22
— Shift every response	6.54	4.48

(b) Legend including euclidean error norm [mm]. (Theoretical minimum in gray)

Figure 5.20: Closed-loop performance when using radial control on the two-angle pyramid.

Figure 5.20 shows the resulting error of the two approaches when shifting the terms in the linearisation in the radial direction according to the radial corrections on the tool. The response model which is shifted is determined using *Def. 3 - Resp. at N_t* . The first approach only shifts the complete response matrix and state evolution by the sum of the control actions in the past, where the second approach shifts every response according to the sum of the optimal control strategy up to that step. Again, the model determined with negative Δv performs better. Also, an improvement can be seen when using the more advanced shifting approach. Figure 5.21 shows the height after each step when every response is shifted and the model is determined using negative Δv. It can be seen that the first wall-angle is initially over-formed, after which the tent-effect forms it back to the target. A sharper wall-angle transition can be observed, which is very close to the target.

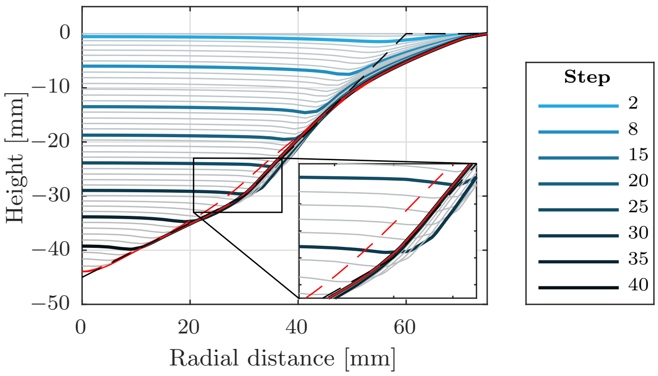

Figure 5.21: Height z_{k+1} after each step k in a corrected analysis using a control model determined with negative Δv and the "Shift every response" approach. The red solid line indicates the final geometry of the controlled analysis and the red dashed line indicates the final geometry of the nominal analysis.

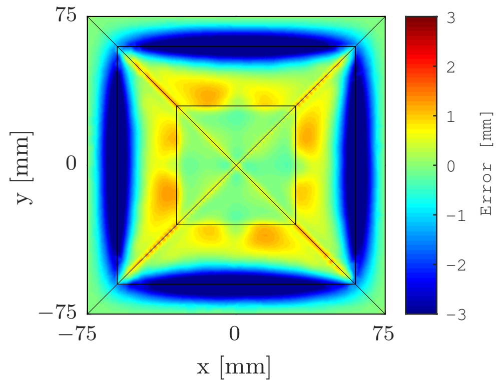

Figure 5.22: Errormap of controlled analysis. The black lines indicate wall angle transitions.

Figure 5.22 shows the error over the whole sheet, to get insight on the actual performance of only applying a correction on the toolpath in the middle of the ribs. It can be observed that the region between the middle of the ribs, where the toolpath is corrected, and the corners contains a larger error. The toolpath is now linearly interpolated between the corrected point and the corners. Another interpolation of the toolpath between the control point and the corner points is expected to yield better results.

5.4.4 Vertical control

While a vertical correction on the complete contour would decrease accuracy in the corners, it is still interesting how the theory developed for the axisymmetric products holds in the case of the tent-effect. In vertical control, radial shift of terms in the linearisation is not required.

Open-loop

Figure 5.23 shows the results of an open-loop run of the MPC using vertical control actions $\Delta \boldsymbol{u}$. In the case of vertical control, *Def. 1 - Full nom. step* can be used without problems. The results of using the MPC in open-loop can be seen in fig. 5.23. The large difference between the actual error using *Def. 1 - Full nom. step* and theoretical minimum as predicted by the MPC indicates a large model error. This can already be expected by looking at the difference between *Def. 3 - Resp. at N_t* (section 5.3.3), which uses the actual effect of a control action, and *Def. 1 - Full nom. step* (section 5.2), which uses the state evolution in a nominal analysis. In chapter 4 on axisymmetric products, the two definitions are more similar.

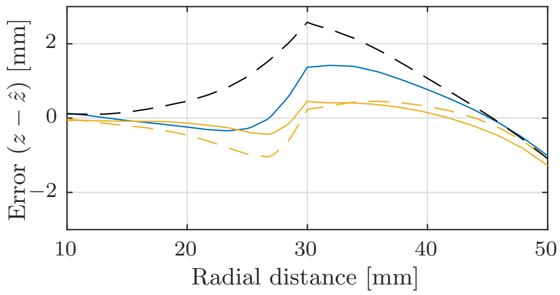

(a) Error from target

Impulse response definition	Assumed control direction: Positive Δu (——)	Assumed control direction: Negative Δu (- - -)
- - No control	17.74	
— 1 - Full nom. step	10.13 (1.09)	
— 3 - Resp. at N_t	5.40 (6.58)	7.13 (6.48)

(b) Legend including euclidean error norm [mm]. (Theoretical minimum in gray)

Figure 5.23: Open-loop performance when using vertical control on the two-angle pyramid.

Def. 3 - Resp. at N_t yields more accurate results, again lower than the theoretical minimum, as was also observed in radial control. Consistent with axisymmetric products, a control model determined with a positive control action Δu yields better results than a control model determined with a negative control action.

Closed-loop

Figure 5.24 shows the results of a closed-loop run of the MPC using vertical control actions $\Delta \boldsymbol{u}$. For *Def. 1 - Full nom. step* an improvement can be seen, where for *Def. 3 - Resp. at N_t* the error is larger than in the open-loop run. The closed-loop run can use *Def. 4 - History aware* to account for the control history, which yields better results than *Def. 3 - Resp. at N_t* . Again, a control model determined using positive Δu gives better results.

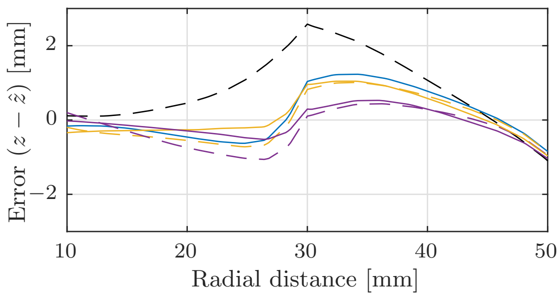

(a) Error from target

Impulse response definition	Assumed control direction: Positive Δu (——)	Assumed control direction: Negative Δu (- - -)
- - No control	17.74	
— 1 - Full nom. step	9.51 (1.09)	
— 3 - Resp. at N_t	7.90 (6.58)	8.71 (6.48)
— 4 - History	5.42 (6.58)	7.74 (6.48)

(b) Legend including euclidean error norm [mm]. (Theoretical minimum in gray)

Figure 5.24: Closed-loop performance when using vertical control on thetwo-angle pyramid.

5.5 Conclusion

In this chapter, it was investigated how the process model can be extended to more complex products. It was shown that the impulse responses in radial control of z-level contours can still be determined using the same theory as used in chapter 4. However, the shape and magnitude is different from the impulse responses seen in vertical control. When the MPC using radial control was tested on Finite Element Simulations, it became clear that the impulse response models should be radially shifted to create an accurate and stable control system. The controller making use of shifted impulse response models was able to reduce the error of over 2 mm due to the tent-effect to values of less than 0.5 mm. This demonstrates that impulse response models in MPC can be used in radial control of z-level contours.

6 | Conclusions and recommendations

In this work, the effect of different linearisation methods on the performance of model predictive control of ISF was investigated. The linearisation methods were studied for a relatively simple target geometry to gain knowledge on the limitations of the linearisations. With that knowledge it is investigated whether the theory can also be applied to more complex geometries. For complex geometries, the matter has been studied in the context of both radial as well as vertical control. The main findings of this work are given below.

6.1 Linearisation around a nominal toolpath

The linearisation used in this thesis differs from previous approaches in control of ISF. Instead of optimizing the complete step height between contours, corrections on this step height are done. This way, more information about the effect of these corrections can be included in the linearisation. This also requires another definition of the impulse response models.

Definition of the impulse response Analyses of the actual effect of a toolpath correction on the geometry of the product indicated that the effect of a correction of the step height is not equal to the effect of the nominal step height. A comparison of geometries was made between products formed by a nominal toolpath and products formed by a corrected toolpath. It was found that the effect of a correction is dependent on the time step at which this difference is observed. In other words, a change in tool path at step k has a different effect on the geometry at step k+1 than on the final geometry of the product. Therefore, a careful consideration should be made in how to define the impulse response. The investigation of consistency of the response over time revealed a limitation of only including the effect of future control actions in the linearisation used in the MPC. A linearisation that includes the effect of control actions in the past was developed and proved to capture some of the changes in the process due to control actions executed, without affecting the complexity of the linearisation, which remains linear.

Linearity of the impulse response One of the main assumptions in using a linearisation in the MPC is that the impulse response does not depend on the magnitude of the control actions. For vertical control, non-linearities with respect to the magnitude of the control action were mainly observed at the outside of the product, where global bending of the product is dominant. This region has been excluded from the analysis by only evaluating a region of interest. In practical applications, global bending will be prevented by the use of additional support, which is expected to eliminate the large non-linearities in the control model.

Another large non-linearity and limitation to existing applications of MPC in Incremental Sheet Forming is the direction of control. Mathematically the direction of the correction on the toolpath can be freely chosen. However, since the state to be controlled is vertical deflection, perpendicular to the flat sheet, only vertical corrections on the toolpath can be applied with success when using impulse response models as defined using the theory in this thesis. The main reason for that is that any control action which is not parallel to the forming direction, will change the location on the product where the deformation occurs. When switching to radial control, which is desirable in more general free-form products, it is required to account for the change of location of deformation in the impulse response models. This expands the simple and efficient QP problem to a general non-linear optimization problem.

6.2 MPC performance

The developed models have been tested on Finite Element simulations of the process. The following aspects of the controller are important when applying Model Predictive Control for Incremental Sheet Forming.

Accuracy In general, the models determined by applying actual corrections in a finite element analysis proved to yield better results than existing models based on nominal path data or a simplified analytical model. *Def. 4 - History aware* that accounts for control actions in the past reduced the error even further, proving that control actions in the past affect the process and should be accounted for during all time steps. However, the use of such more detailed process models comes at the cost of a large increase of computational cost for determining these models.

Range of validity The MPC proved to work well for target geometries which are similar to that of the nominal analysis. The linearisation developed can also be used to predict the nominal state evolution of a closely related geometry, but limits the freedom of choosing a desirable toolpath.

For future perspectives, it is desirable that the models proposed in this thesis do not have to be determined again using computationally expensive finite element analyses. The relations with product target geometry and process parameters such as tool and sheet size and material should be established to make the models more general. In this work it was observed that responses are often very similar for closely related steps. It is recommended that the use of smart interpolation or more advanced machine learning techniques is explored to determine the response models for closely related processes.

Robustness Tests of the MPC in a numerical environment proved that the MPC can deal with small changes in process parameters. This does however not guarantee success when the MPC is tested on a real stochastic process where parameters can vary over the sheet and other unknown modelling errors will be present. Especially important in robustness is the compliance of the setup, which can cause a large error and requires large deviations from the toolpath. The MPC proved to be able to deal with this source of error well.

It is recommended that the working of the MPC is tested on a real ISF setup to ensure stability of the MPC and robustness to stochastic parameter variation and other sources of uncertainty.

Two-sidedness of the linearisation In an attempt to improve the accuracy of the linearisation, the state evolution resulting from the nominal path and the effect of control actions has been split, where in many other research applications, these two are assumed to be equal. This results in a two-sided problem for the MPC, where both positive and negative corrections on the toolpath are possible. In this work, the effect of positive and negative directions were not simultaneously implemented in the process model. A direction of correcting was assumed and the corresponding model was used in the process model for the MPC. It was shown that the choice of an assumed direction of the corrections has a significant effect on the performance of the MPC controller.

For further research, it is recommended to look into the possibility of extending the MPC to a non-linear formulation in which a different control model can be used for positive and negative control actions simultaneously.

Bibliography

[1] K. Schwab and W. E. Forum, *The Fourth Industrial Revolution.* World Economic Forum, 2016.

[2] M.-Z. Li, Z.-Y. Cai, and C.-G. Liu, “Flexible manufacturing of sheet metal parts based on digitized-die,” *Robotics and Computer-Integrated Manufacturing*, vol. 23, no. 1, pp. 107–115, 2007.

[3] W. C. Emmens, G. Sebastiani, and A. H. van den Boogaard, “The technology of Incremental Sheet Forming-A brief review of the history,” *Journal of Materials Processing Technology*, vol. 210, no. 8, pp. 981–997, 2010.

[4] J. Jeswiet, F. Micari, G. Hirt, A. Bramley, J. Duflou, and J. Allwood, “Asymmetric single point incremental forming of sheet metal,” *CIRP Annals - Manufacturing Technology*, vol. 54, no. 2, pp. 88–114, 2005.

[5] J. R. Duflou, A. M. Habraken, J. Cao, R. Malhotra, M. Bambach, D. Adams, H. Vanhove, A. Mohammadi, and J. Jeswiet, “Single point incremental forming: state-of-the-art and prospects,” *International Journal of Material Forming*, vol. 11, no. 6, pp. 743–773, 2018.

[6] G. Ambrogio, E. Sgambitterra, L. De Napoli, F. Gagliardi, G. Fragomeni, A. Piccininni, P. Gugleilmi, G. Palumbo, D. Sorgente, L. La Barbera, and T. M. Villa, “Performances Analysis of Titanium Prostheses Manufactured by Superplastic Forming and Incremental Forming,” *Procedia Engineering*, vol. 183, pp. 168–173, 2017.

[7] M. Amino, M. Mizoguchi, Y. Terauchi, and T. Maki, “Current status of ”Dieless” Amino’s incremental forming,” *Procedia Engineering*, vol. 81, no. October, pp. 54–62, 2014.

[8] G. Hirt, M. Bambach, W. Bleck, U. Prahl, and J. Stollenwerk, “The Development of Incremental Sheet Forming from Flexible Forming to Fully Integrated Production of Sheet Metal Parts,” in *Advances in Production Technology*, no. January, pp. 117–129, Springer, 2015.

[9] H. Lu, M. Kearney, Y. Li, S. Liu, W. J. Daniel, and P. A. Meehan, “Model predictive control of incremental sheet forming for geometric accuracy improvement,” *International Journal of Advanced Manufacturing Technology*, vol. 82, no. 9-12, pp. 1781–1794, 2016.

[10] H. Ren, J. Xie, S. Liao, D. Leem, K. Ehmann, and J. Cao, “In-situ springback compensation in incremental sheet forming,” *CIRP Annals*, vol. 68, no. 1, pp. 317–320, 2019.

[11] R. Neugebauer, T. Altan, M. Geiger, M. Kleiner, and A. Sterzing, “Sheet metal forming at elevated temperatures,” *CIRP Annals - Manufacturing Technology*, vol. 55, no. 2, pp. 793–816, 2006.

[12] J. R. Duflou, B. Callebaut, J. Verbert, and H. De Baerdemaeker, “Laser assisted incremental forming: Formability and accuracy improvement,” *CIRP Annals - Manufacturing Technology*, vol. 56, no. 1, pp. 273–276, 2007.

[13] G. Fan, L. Gao, G. Hussain, and Z. Wu, “Electric hot incremental forming: A novel technique,” *International Journal of Machine Tools and Manufacture*, vol. 48, no. 15, pp. 1688–1692, 2008.

[14] M. Bambach, B. Taleb Araghi, and G. Hirt, “Strategies to improve the geometric accuracy in asymmetric single point incremental forming,” *Production Engineering*, vol. 3, no. 2, pp. 145–156, 2009.

[15] G. Hirt, J. Ames, M. Bambach, R. Kopp, and R. Kopp, "Forming strategies and process modelling for CNC incremental sheet forming," *CIRP Annals - Manufacturing Technology*, vol. 53, no. 1, pp. 203–206, 2004.

[16] A. Fiorentino, G. C. Feriti, C. Giardini, and E. Ceretti, "Part precision improvement in incremental sheet forming of not axisymmetric parts using an artificial cognitive system," *Journal of Manufacturing Systems*, vol. 35, pp. 215–222, 2015.

[17] A. Fiorentino, G. C. Feriti, E. Ceretti, and C. Giardini, "Capability of iterative learning control and influence of the material properties on the improvement of the geometrical accuracy in incremental sheet forming process," *International Journal of Material Forming*, vol. 11, no. 1, pp. 125–134, 2018.

[18] J. D. Fischer, M. R. Woodside, M. M. Gonzalez, N. A. Lutes, D. A. Bristow, and R. G. Landers, "Iterative learning control of single point incremental sheet forming process using digital image correlation," *Procedia Manufacturing*, vol. 34, pp. 940–949, 2019.

[19] A. K. Behera, J. Verbert, B. Lauwers, and J. R. Duflou, "Tool path compensation strategies for single point incremental sheet forming using multivariate adaptive regression splines," *CAD Computer Aided Design*, vol. 45, no. 3, pp. 575–590, 2013.

[20] J. M. Allwood, S. R. Duncan, J. Cao, P. Groche, G. Hirt, B. Kinsey, T. Kuboki, M. Liewald, A. Sterzing, and A. E. Tekkaya, "Closed-loop control of product properties in metal forming," *CIRP Annals - Manufacturing Technology*, vol. 65, no. 2, pp. 573–596, 2016.

[21] A. Mesbah, "Stochastic model predictive control: An overview and perspectives for future research," *IEEE Control Systems*, vol. 36, no. 6, pp. 30–44, 2016.

[22] J. A. Polyblank, J. M. Allwood, and S. R. Duncan, "Closed-loop control of product properties in metal forming: A review and prospectus," *Journal of Materials Processing Technology*, vol. 214, no. 11, pp. 2333–2348, 2014.

[23] J. M. Allwood, O. Music, A. Raithathna, and S. R. Duncan, "Closed-loop feedback control of product properties in flexible metal forming processes with mobile tools," *CIRP Annals*, vol. 58, pp. 287–290, jan 2009.

[24] H. Wang and S. R. Duncan, "Model Predictive Based Incremental Sheet Forming Toolpath Optimisation," in *UKACC International Conference on control*, 2010.

[25] A. He, M. P. Kearney, K. J. Weegink, C. Wang, S. Liu, and P. A. Meehan, "A model predictive path control algorithm of single-point incremental forming for non-convex shapes," *International Journal of Advanced Manufacturing Technology*, vol. 107, no. 1-2, pp. 123–143, 2020.

[26] A. He, C. Wang, S. Liu, and P. A. Meehan, "Switched model predictive path control of incremental sheet forming for parts with varying wall angles," *Journal of Manufacturing Processes*, vol. 53, no. October 2019, pp. 342–355, 2020.

[27] O. Music and J. M. Allwood, "The use of spatial impulse responses to characterise flexible forming processes with mobile tools," *Journal of Materials Processing Technology*, vol. 212, no. 5, pp. 1139–1156, 2012.

[28] H. Lu, "Investigation of Control of the Incremental Forming Processes," 2016.

[29] Z. Pan, "Chatter analysis of robotic machining process Zengxi," *Journal of Materials Processing Technology*, vol. 173, pp. 301–309, 2006.

[30] U. Schneider, M. Momeni-K, M. Ansaloni, and A. Verl, "Stiffness modeling of industrial robots for deformation compensation in machining," *IEEE International Conference on Intelligent Robots and Systems*, no. Iros, pp. 4464–4469, 2014.

[31] L. Sun and L. Fang, "An approximation method for stiffness calculation of robotic arms with hybrid open- and closed-loop kinematic chains," *Advances in Mechanical Engineering*, vol. 10, no. 2, pp. 1–12, 2018.

Appendices

A | Finite Element Model

The Finite Element model built to obtain control models and test the MPC performance has been made in commercial finite element package Abaqus. The model consists of a shell-meshed sheet and rigid tool. The sheet is fixed in all DOF on its edges and the tool has prescribed displacement boundary conditions, but a fixed rotation. The sheet is meshed with approximately 4500 linear quadrilateral reduced integration shell elements (Abaqus S4R) with 5 integration points through thickness. The contact area was meshed using a spacing of 1.75 mm with surrounding regions being coarser. The contact between the tool and the sheet was modelled with "Hard" contact in normal direction and the penalty method friction formulation in tangential direction. The maximum time step taken is $\Delta t = 0.03$ s and the toolspeed is $v = 30$ mm/s.

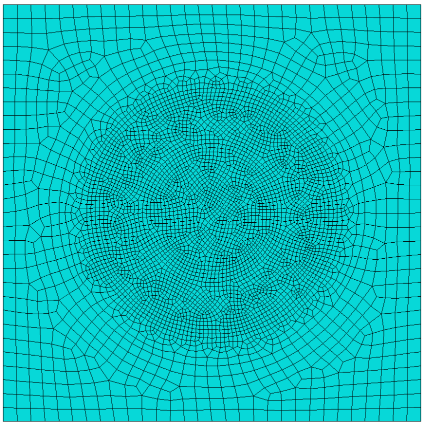

Figure A.1: Axisymmetric products mesh

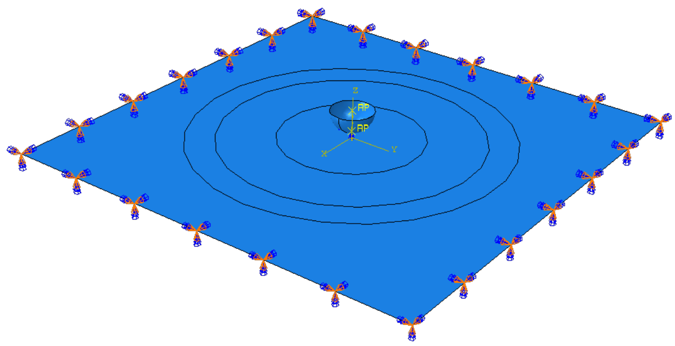

Figure A.2: Sheet boundary conditions

In all models, the aluminium alloy AlMg3 has been used. The material has been modelled using a simple power law:

$$\sigma = C\varepsilon^n \tag{A.1}$$

With $C = 390$ and $n = 0.19$ for AlMg3 [27]

B | Process model

B.1 Time evolving formulation

Simulations of applying control steps Δu_k learned that the effect of control step Δu_k on the next state $\boldsymbol{z}_{k+1}$ is not equal to the effect on the final state $\boldsymbol{z}_{N_t}$. To account for this evolution over time, it is desirable that when the process is linearised at step k, not only the corrections of the coming steps in the process are accounted for $(k, k+1, \ldots, N_t)$, but also the corrections which were already performed in the past $(1, 2, \ldots, k-1)$. The effect of all control actions in the system $(1, 2, , \ldots, N_t)$ will be stored in time-variant matrix $\boldsymbol{Q}_k$. The matrix is time-variant since the effect of a control actions on a certain step is "removed" from the matrix when the step is performed. When the linearisation is evaluated at time step k using $\boldsymbol{Q}_k$, columns $\boldsymbol{q}_l \in \boldsymbol{Q}_k$ are defined by:

$$\boldsymbol{q}_l = \frac{\boldsymbol{z}_{N_t}(\Delta u_l) - \boldsymbol{z}_k(\Delta u_l)}{\Delta u_l} - \frac{\bar{\boldsymbol{z}}_{N_t} - \bar{\boldsymbol{z}}_k}{\Delta u_l} \tag{B.1}$$

In words: the column $\boldsymbol{q}_l$ will describe what the change to the process from step k until the final step is as a result of a control action Δu_l at step l. The final geometry can now be predicted by:

$$\tilde{\boldsymbol{z}}_{N_t} = \boldsymbol{z}_k + \bar{\boldsymbol{z}}_{N_t} - \bar{\boldsymbol{z}}_k + \sum_{l=1}^{N_t} \boldsymbol{q}_l \Delta u_l \tag{B.2}$$

More conveniently written in matrix-vector notation as:

$$\tilde{\boldsymbol{z}}_{N_t} = \boldsymbol{z}_k + \bar{\boldsymbol{z}}_{N_t} - \bar{\boldsymbol{z}}_k + \boldsymbol{Q}_k \boldsymbol{\Delta u} \tag{B.3}$$

With $\boldsymbol{\Delta u}$ containing all $N_t - 1$ corrections on the toolpath. For use in an optimization algorithm, the optimization variables $\Delta \boldsymbol{u}_{opt,k} = [\Delta u_k, \Delta u_{k+1}, \ldots, \Delta u_{N_t-1}]^T$ should be split from the influence of control steps which are already performed $\boldsymbol{\Delta u}_{his,k} = [\Delta u_1, \Delta u_2, \ldots, \Delta u_{k-1}]^T$. In the same fashion, $\boldsymbol{Q}_{his,k}$ and $\boldsymbol{Q}_{opt,k}$ are the corresponding subsets of $\boldsymbol{Q}_k$.

$$\begin{aligned} \tilde{\boldsymbol{z}}_{N_t} &= \boldsymbol{z}_k + \bar{\boldsymbol{z}}_{N_t} - \bar{\boldsymbol{z}}_k + \boldsymbol{Q}_k \Delta \boldsymbol{u} & \text{(B.4)} \\ &= \boldsymbol{z}_k + \bar{\boldsymbol{z}}_{N_t} - \bar{\boldsymbol{z}}_k + \boldsymbol{Q}_{his,k} \Delta \boldsymbol{u}_{his,k} + \boldsymbol{Q}_{opt,k} \Delta \boldsymbol{u}_{opt,k} & \text{(B.5)} \end{aligned}$$

B.2 QP formulation

When the optimization problem only contains quadratic terms, it can be converted to a standard QP formulation and be solved efficiently with standard QP optimization techniques:

$$J = \|\boldsymbol{z}_k + \bar{\boldsymbol{z}}_{N_t} - \bar{\boldsymbol{z}}_k + \boldsymbol{G}_k \Delta \boldsymbol{u}_k - \hat{\boldsymbol{z}}_{N_t}\|_2 + \alpha \|\Delta \boldsymbol{u}_k\|_2 \tag{B.6}$$

$$= \Delta \boldsymbol{u}_k^T (\boldsymbol{G}_k^T \boldsymbol{G}_k + \alpha \boldsymbol{I}) \Delta \boldsymbol{u}_k + 2(\boldsymbol{z}_k + \bar{\boldsymbol{z}}_{N_t} - \bar{\boldsymbol{z}}_k - \hat{\boldsymbol{z}}_{N_t}) \boldsymbol{G}_k \Delta \boldsymbol{u}_k \tag{B.7}$$

$$= \frac{1}{2} \Delta \boldsymbol{u}_k^T 2(\boldsymbol{G}_k^T \boldsymbol{G}_k + \alpha \boldsymbol{I}) \Delta \boldsymbol{u}_k + 2(\boldsymbol{z}_k + \bar{\boldsymbol{z}}_{N_t} - \bar{\boldsymbol{z}}_k - \hat{\boldsymbol{z}}_{N_t}) \boldsymbol{G}_k \Delta \boldsymbol{u}_k \tag{B.8}$$

Note that this is not the real representation of an euclidean or L2 norm, which should include a square root of the terms. The QP formulation leads to the following optimization problem:

$$\begin{aligned} \underset{\Delta \boldsymbol{u}_k}{\text{minimize}} \quad & \frac{1}{2} \Delta \boldsymbol{u}_k^T \boldsymbol{H} \Delta \boldsymbol{u}_k + \boldsymbol{f}^T \Delta \boldsymbol{u}_k \\ \text{subject to} \quad & \boldsymbol{H} = 2(\boldsymbol{G}_k^T \boldsymbol{G}_k + \alpha \boldsymbol{I}), \\ & \boldsymbol{f}^T = 2(\boldsymbol{z}_k + \bar{\boldsymbol{z}}_{N_t} - \bar{\boldsymbol{z}}_k - \hat{\boldsymbol{z}}_{N_t}) \boldsymbol{G}_k, \\ & lb \leq \Delta u_i \leq ub \quad \forall\, i \end{aligned} \tag{B.9}$$

This problem can be solved efficiently using MATLAB function *quadprog* from the optimization toolbox and is fast enough for on-line control.

When *Def. 4 - History aware* is used, the extra term $\boldsymbol{Q}_{his,k} \Delta \boldsymbol{u}_{his,k}$ is added to $\boldsymbol{f}^T$.

C Spatially invariance of axisymmetric products

In this thesis, the height of the product is sampled over the radius at a series of angle around the circumference and then averaged. To justify the averaging, the response should be consistent over the angles around the circumference. The biggest concern in ISF is the effect of the clamping. When the clamp is rectangular and a circular product is made, the distance to the clamp is not equal over the whole circumference, giving another stiffness at the locations close to the corners than at the locations close to the edge. fig. C.1 shows two different samplings of the cup. The left one is sampled at the locations close to the edges where the right one is sampled in the corners.

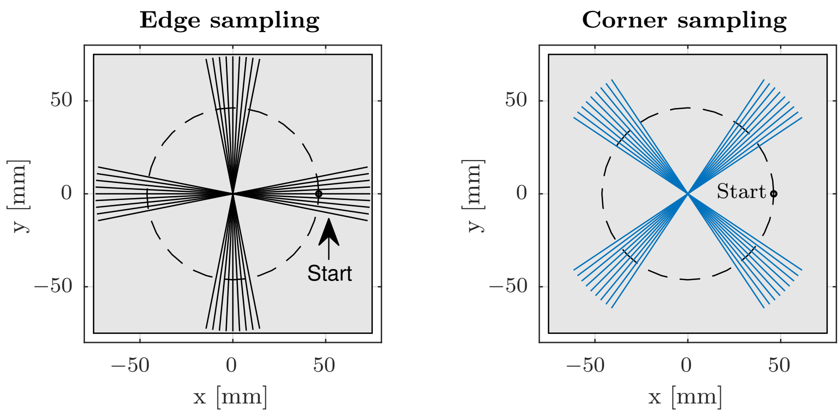

Figure C.1: Angular sampling cases

Figure C.2 shows that there is some difference in the response in the first few contours. This is the region with low stiffness where global bending is dominant. When the process becomes more constant, the difference between the two samplings is negligible. It can therefore be assumed that the impulse response of this geometry is spatially invariant and can therefore be used as a control model.

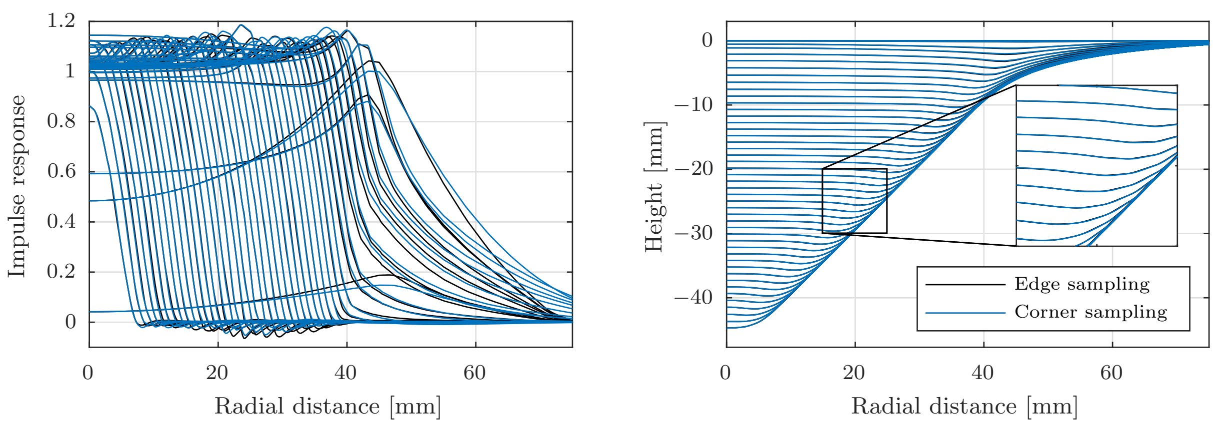

Figure C.2: Difference between height of the contour and spatial impulse response for different angular samples (fig. C.1).

D Time-consistency complex products

Similar to the analysis of the response of a control action over time for an axisymmetric product in section 4.3.2, the same can be done for the complex products in chapter 5. This yields the following result:

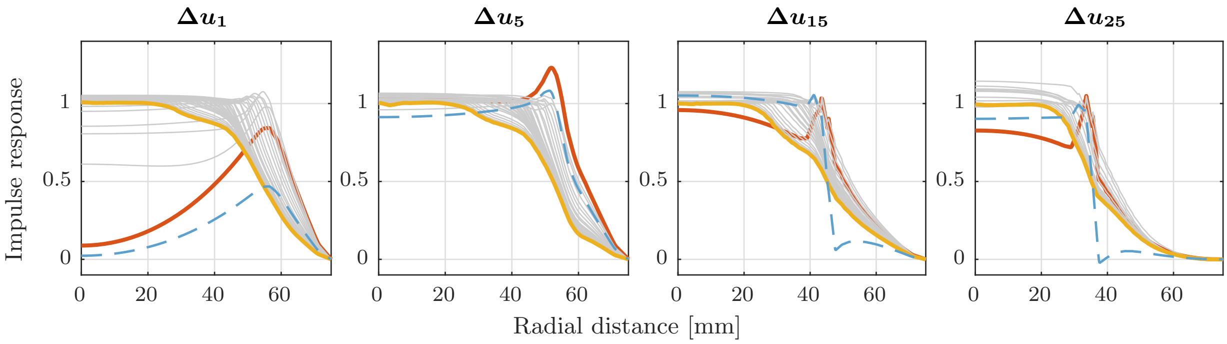

a) Model determined with $\Delta u = 0.5$ mm

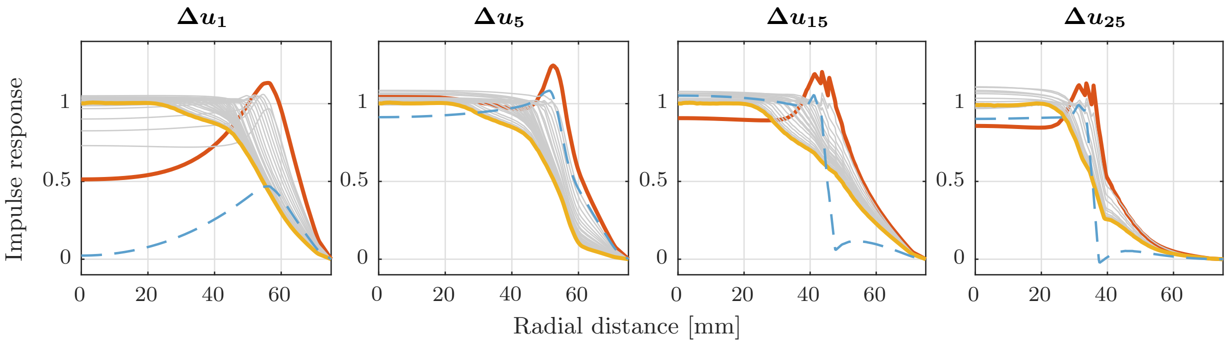

b) Model determined with $\Delta u = -0.5$ mm

Figure D.1: Evolution of the impulse response determined with $\Delta u = \pm 0.5$ mm from step k (— Def. 2) to step $N_t - 1$ (— Def. 3). The responses between those steps can be seen in gray. As a reference, *Def. 1 - Full nom. step* is included as the dashed line (- -).

E MPC control actions

In this appendix, the results of the MPC tests in chapter 4 and chapter 5 are given. The figures on the left give the value of control action Δu or Δv at every step. The figures on the right give the cumulative value of the values in the left figures. As the step height between the contours is optimized instead of the location of the contour in space, the cumulative value of the control actions indicates how far the corrected toolpath deviated from the original toolpath.

E.1 Axisymmetric products

The following section contains the results from chapter 4. In this chapter, only vertical corrections Δu are done.

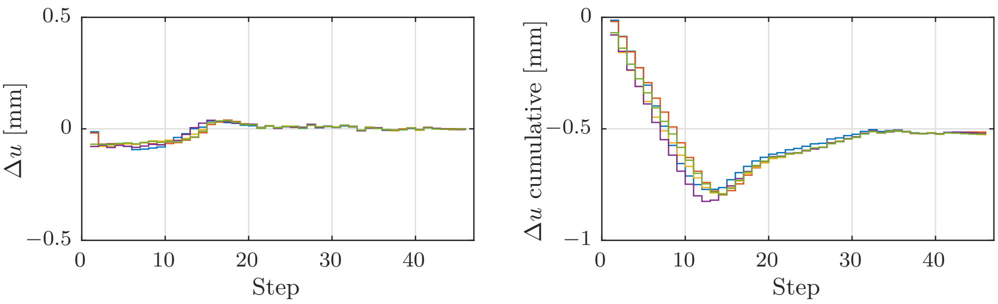

a) Models defined by applying a positive Δu

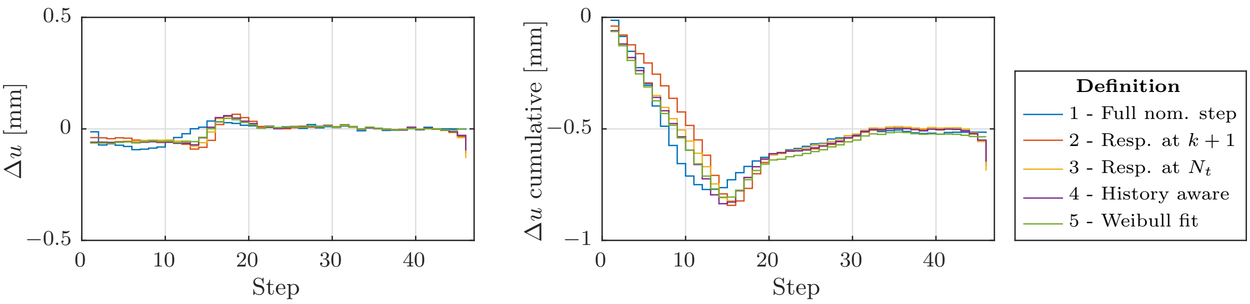

b) Models defined by applying a negative Δu

Figure E.1: Control actions applied in closed-loop control of the straight cone in section 4.4.3

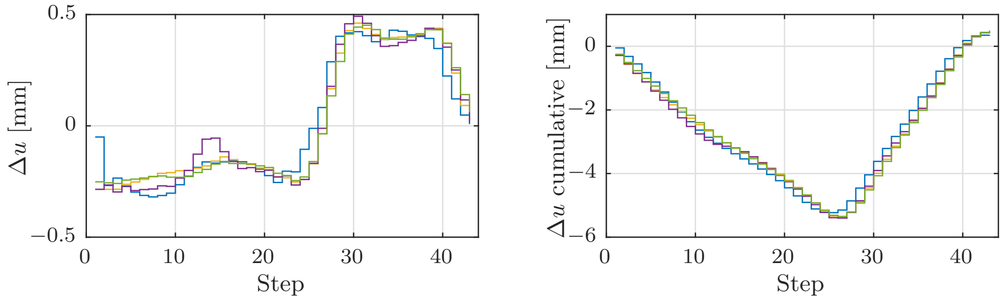

a) Models defined by applying a positive Δu

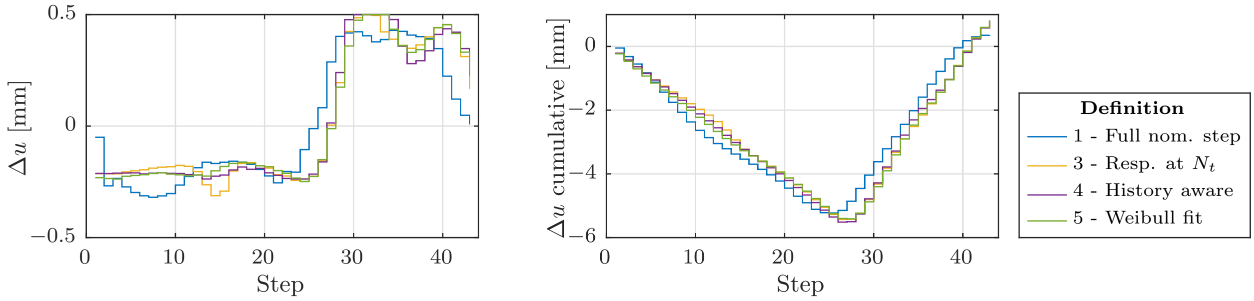

b) Models defined by applying a negative Δu

Figure E.2: Control actions applied in closed-loop control of the one-step cone using a new target in section 4.4.5

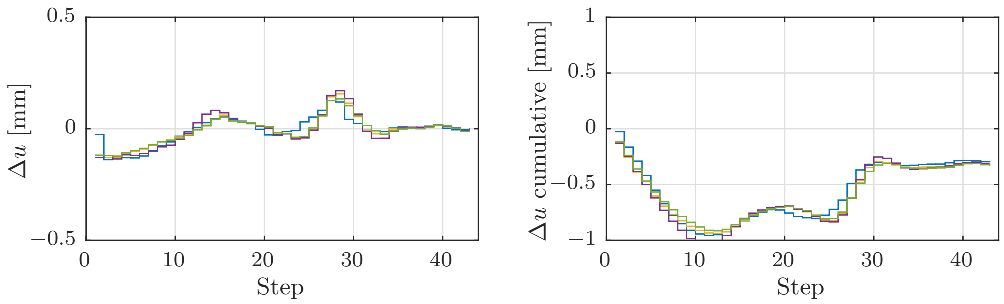

a) Models defined by applying a positive Δu

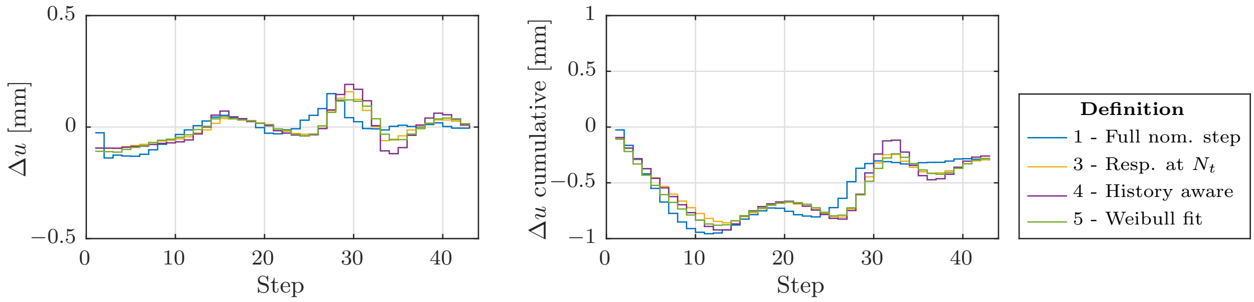

b) Models defined by applying a negative Δu

Figure E.3: Control actions applied in closed-loop control of the one-step cone using a new target and an approximated state evolution in section 4.4.5

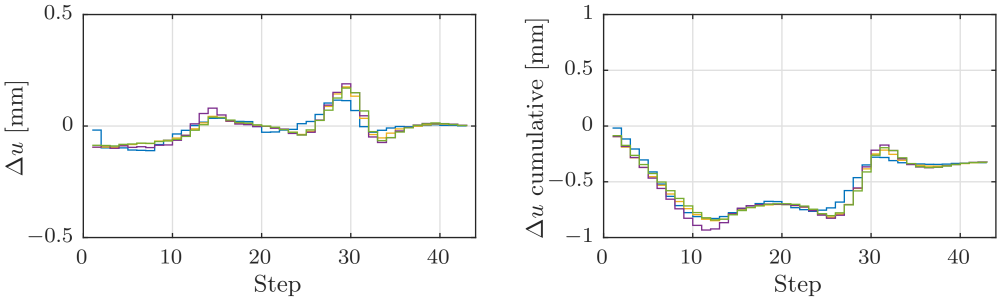

a) Models defined by applying a positive Δu

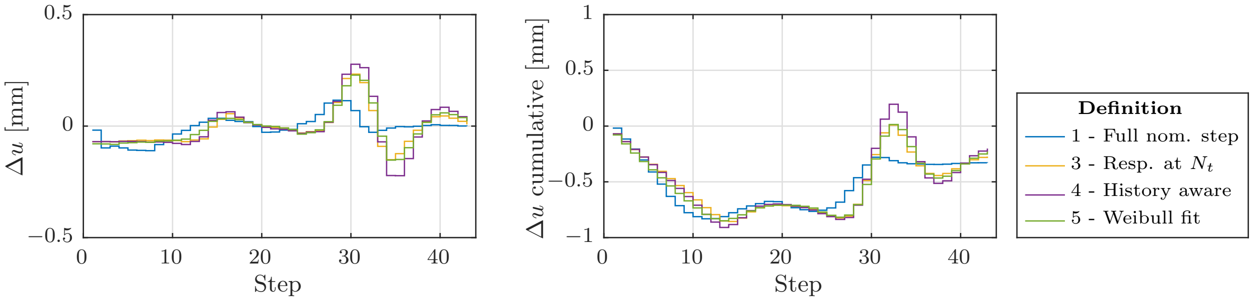

b) Models defined by applying a negative Δu

Figure E.4: Control actions applied in closed-loop control of the one-step cone using a new target and exact state evolution in section 4.4.5

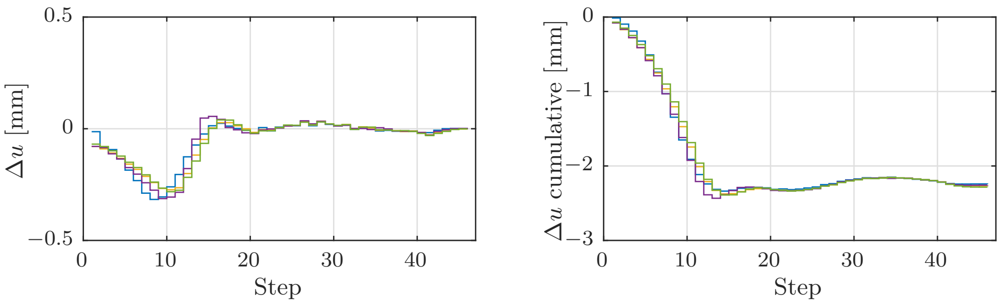

a) Models defined by applying a positive Δu

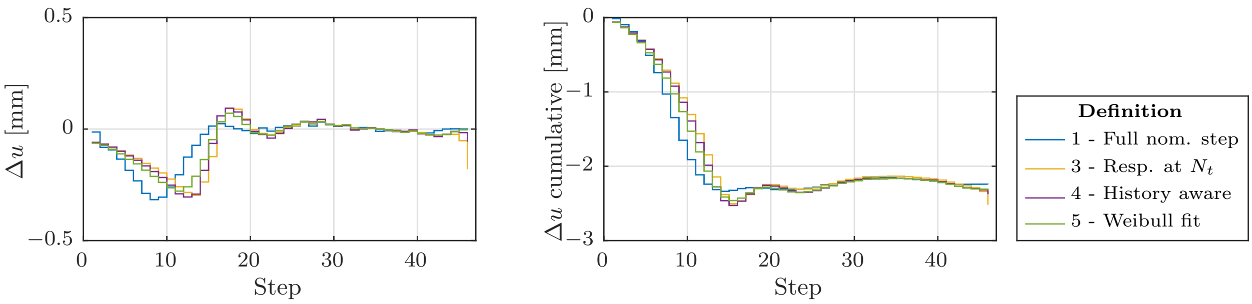

b) Models defined by applying a negative Δu

Figure E.5: Control actions applied in the closed-loop robustness against compliance test in section 4.4.4

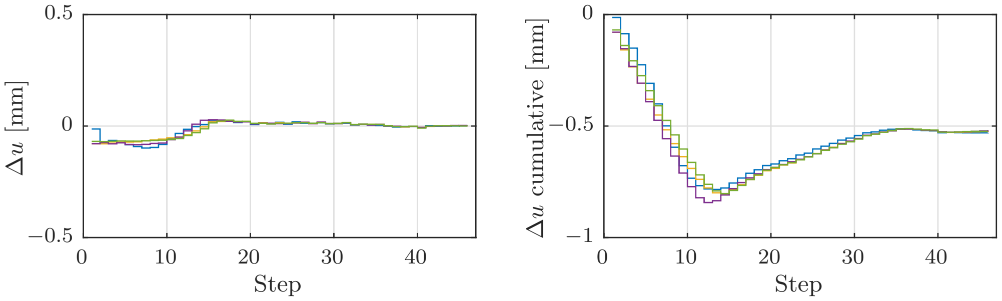

a) Models defined by applying a positive Δu

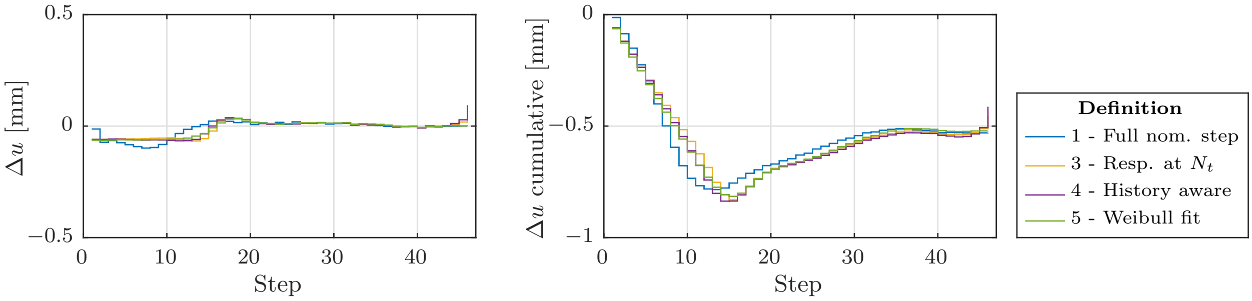

b) Models defined by applying a negative Δu

Figure E.6: Control actions applied in the closed-loop robustness against random parameter set 1 test in section 4.4.4

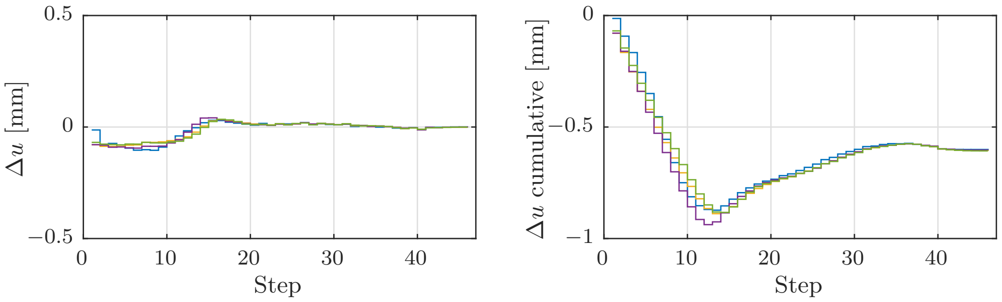

a) Models defined by applying a positive Δu

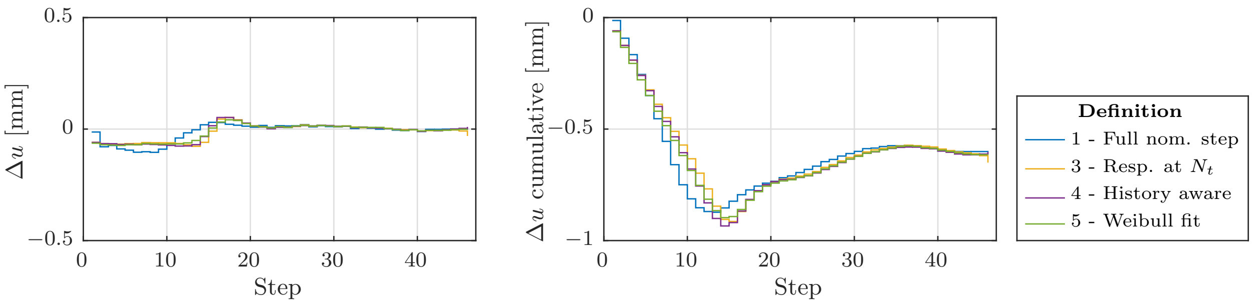

b) Models defined by applying a negative Δu

Figure E.7: Control actions applied in the closed-loop robustness against random parameter set 2 test in section 4.4.4

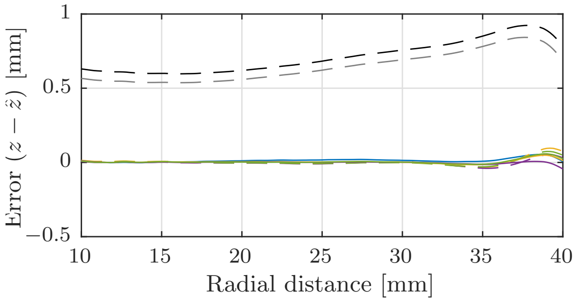

(a) Error from target

Impulse response definition	Assumed control direction: Positive Δu (——)	Negative Δu (- - -)
- - Nominal parameters	8.03	
- - Random parameters	8.84	
— 1 - Full nom. step	0.22 (0.12)	
— 3 - Resp. at N_t	0.16 (0.12)	0.31 (0.10)
— 4 - History	0.08 (0.12)	0.21 (0.10)
— 5 - Weibull fit	0.19 (0.12)	0.25 (0.12)

(b) Legend including euclidean error norm [mm]. (Theoretical minimum in gray)

Figure E.8: Robustness to random parameter set 2 in closed-loop.

E.2 Complex products

The following section contains the results from chapter 5. For these complex products, both radial and vertical control is applied.

E.2.1 Radial control actions

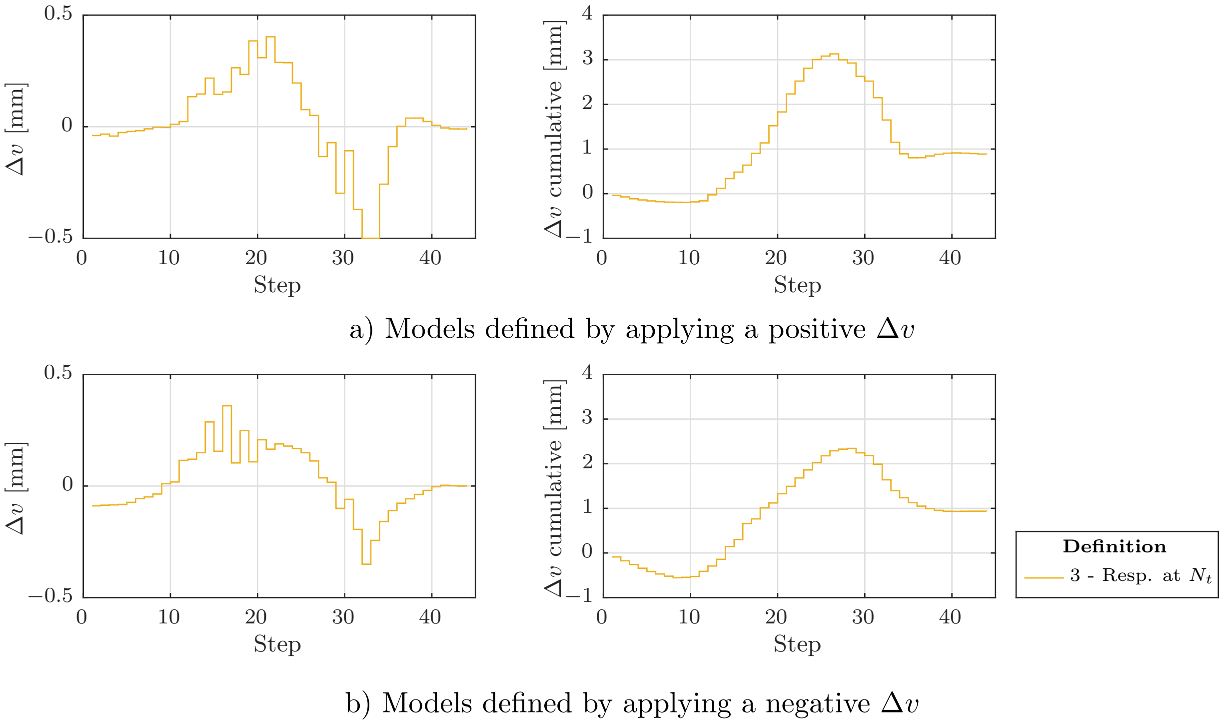

Figure E.9: Control actions applied in radial open-loop control of the two-angle pyramid in section 5.4.3

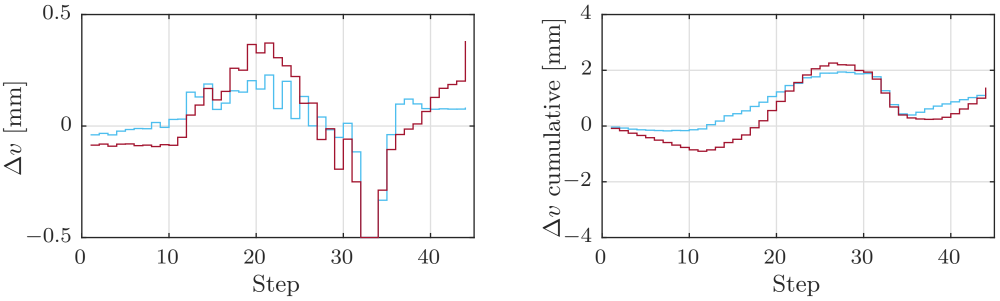

a) Models defined by applying a positive Δv

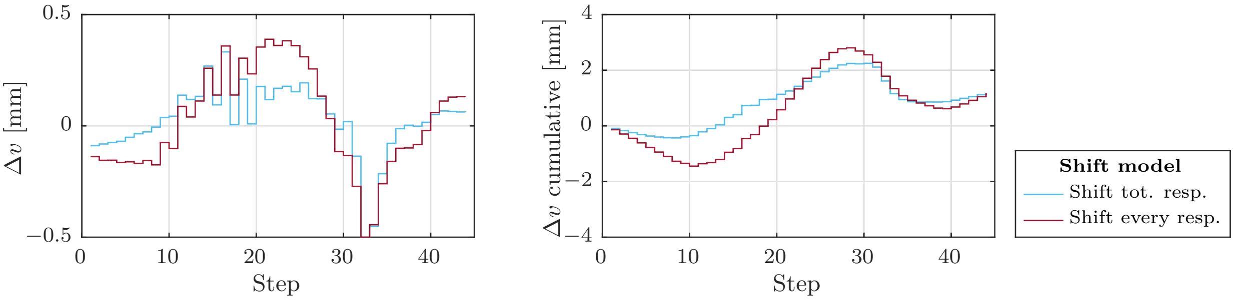

b) Models defined by applying a negative Δv

Figure E.10: Control actions applied in radial closed-loop control of the two-angle pyramid in section 5.4.3

E.3 Vertical control actions

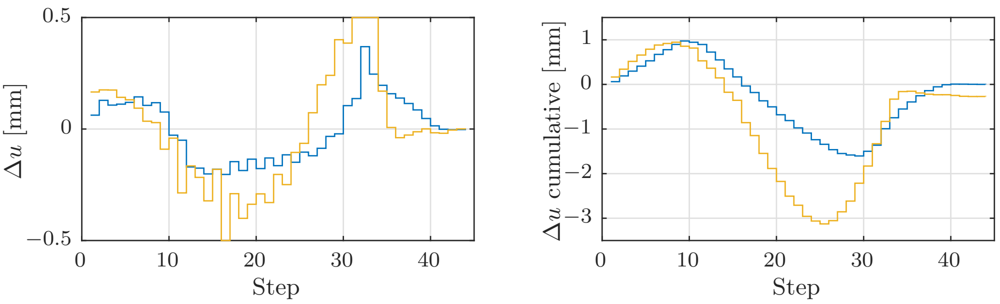

a) Models defined by applying a positive Δu

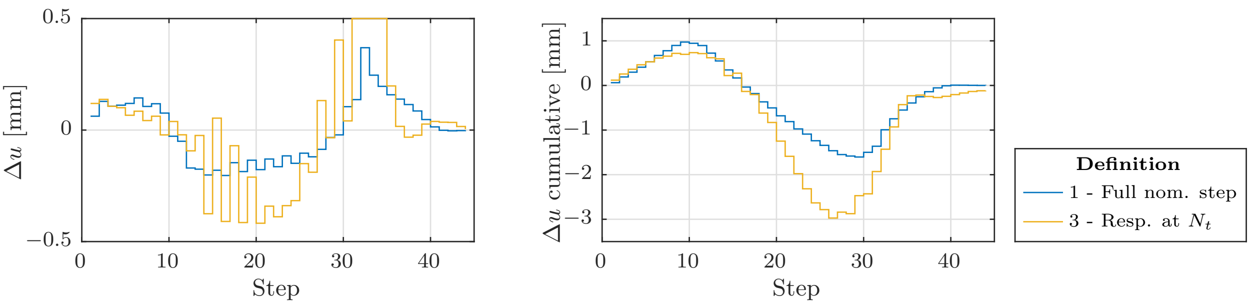

b) Models defined by applying a negative Δu

Figure E.11: Control actions applied in vertical open-loop control of the two-angle pyramid in section 5.4.4

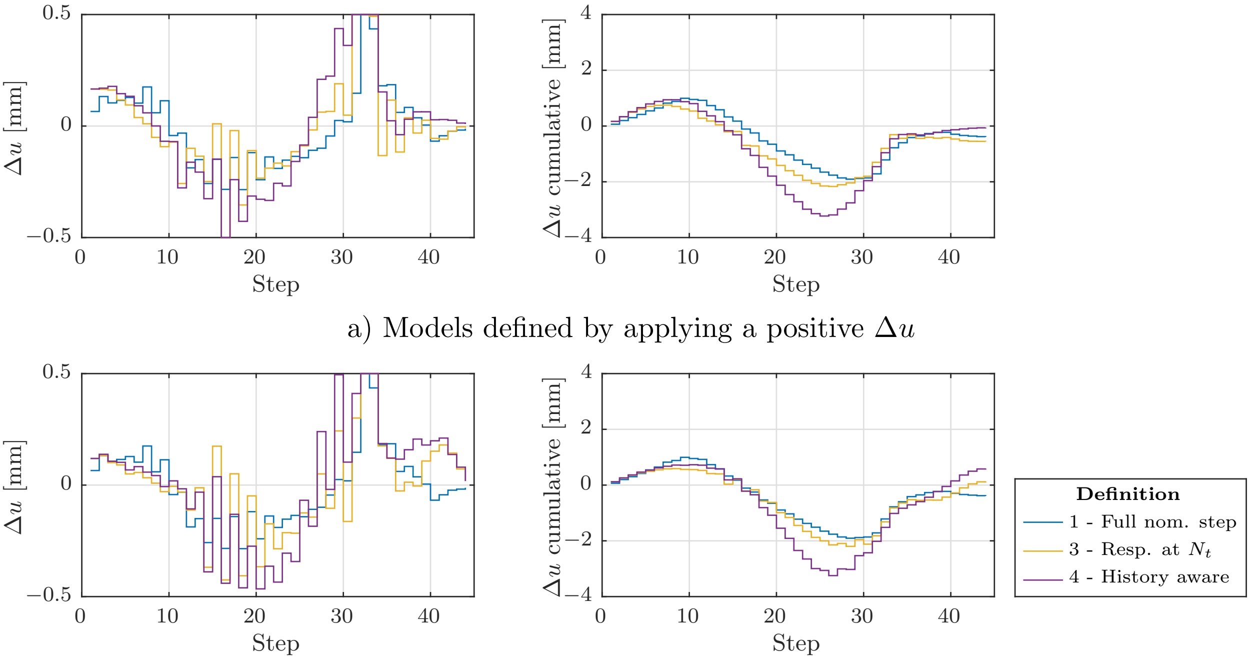

b) Models defined by applying a negative Δu

Figure E.12: Control actions applied in vertical closed-loop control of the two-angle pyramid in section 5.4.4

F Plagiarism report

The thesis has been scanned for plagiarism by TurnItIn. No significant similarities were found, as can be seen below. The full report can be requested from the author.

turnitin

Master thesis Dylan Sikkelbein - plagiarism scan.pdf
Jan 18, 2021
24833 words / 115158 characters

Dylan Sikkelbein

Master thesis Dylan Sikkelbein - plagiarism scan.pdf

Sources Overview

1%

OVERALL SIMILARITY

1	Javier Segurado, Ricardo A. Lebensohn, Javier LLorca. "Computational Homogenization of Polycrystals", Elsevier BV, 2018 CROSSREF	<1%
2	Omer Music, Julian M. Allwood. "The use of spatial impulse responses to characterise flexible forming processes with mobile tools", J... CROSSREF	<1%
3	espace.library.uq.edu.au INTERNET	<1%
4	J.M. Allwood, S.R. Duncan, J. Cao, P. Groche, G. Hirt, B. Kinsey, T. Kuboki, M. Liewald, A. Sterzing, A.E. Tekkaya. "Closed-loop control of ... CROSSREF	<1%
5	Yanle Li, Xiaoxiao Chen, Zhaobing Liu, Jie Sun, Fangyi Li, Jianfeng Li, Guoqun Zhao. "A review on the recent development of incremental... CROSSREF	<1%
6	digital.lib.washington.edu INTERNET	<1%
7	mafiadoc.com INTERNET	<1%
8	repository.tudelft.nl INTERNET	<1%
9	floatingsolarchimney.gr INTERNET	<1%

Excluded search repositories:

- None

Excluded from Similarity Report:

- Bibliography
- Quotes
- Citations
- Small Matches (less than 12 words).

Excluded sources:

- None